



HAL
open science

Synthesis, characterization and separation of chiral and achiral diastereomers of Schiff base Pd(II) complex: A comparative study of their DNA- and HSA-binding

Zahra Kazemi, Hadi Amiri Rudbari, Mehdi Sahihi, Valiollah Mirkhani, Majid Moghadam, Sharam Tangestaninejad, Iraj Mohammadpoor-Baltork, Gholamhassan Azimi, Sajjad Gharaghani, Abolghasem Abbasi Kajani

► To cite this version:

Zahra Kazemi, Hadi Amiri Rudbari, Mehdi Sahihi, Valiollah Mirkhani, Majid Moghadam, et al.. Synthesis, characterization and separation of chiral and achiral diastereomers of Schiff base Pd(II) complex: A comparative study of their DNA- and HSA-binding. *Journal of Photochemistry and Photobiology B: Biology*, 2016, 163, pp.246-260. 10.1016/j.jphotobiol.2016.08.035 . hal-04087491

HAL Id: hal-04087491

<https://uca.hal.science/hal-04087491>

Submitted on 3 May 2023

HAL is a multi-disciplinary open access archive for the deposit and dissemination of scientific research documents, whether they are published or not. The documents may come from teaching and research institutions in France or abroad, or from public or private research centers.

L'archive ouverte pluridisciplinaire **HAL**, est destinée au dépôt et à la diffusion de documents scientifiques de niveau recherche, publiés ou non, émanant des établissements d'enseignement et de recherche français ou étrangers, des laboratoires publics ou privés.



Distributed under a Creative Commons Attribution - NonCommercial - NoDerivatives 4.0 International License

Synthesis, characterization and separation of chiral and achiral diastereomers of Schiff base Pd(II) complex: A comparative study of their DNA- and HSA-binding

Zahra Kazemi ^a, Hadi Amiri

Rudbari ^a, Mehdi Sahihi ^a, Valiollah Mirkhani ^a, Majid Moghadam ^a, Sharam Tangestaninejad ^a, Iraj Mohammadpoor-Baltork ^a, Gholamhassan Azimi ^a, Sajjad Gharaghani ^b, Abolghasem Abbasi Kajani ^c

^a

Department of Chemistry, University of Isfahan, Isfahan 81746-73441, Iran

^b

Department of Bioinformatics, Laboratory of Bioinformatics and Drug Design, Institute of Biochemistry and Biophysics, University of Tehran, Tehran, Iran

^c

Department of Biotechnology, Faculty of Advanced Sciences and Technologies, University of Isfahan, Isfahan, Iran

Abstract

A racemic mixture of a new chiral Schiff base ligand (**HL**: *R/S*-(1-phenylethylimino)methylnaphtalen-2-ol) has been utilized to prepare Pd(II) complex. Crystallization technique has been employed to separate diastereomeric pairs of Pd(II) complex: (*meso***PdL₂**) and (*rac***PdL₂**) that in this paper are known as **PdL₂¹** and **PdL₂²**, respectively. The synthesized complexes have been characterized by means of elemental analysis (CHN), FT-IR, ¹H and ¹³C NMR spectroscopies. Moreover, **PdL₂¹** has been structurally characterized by single-crystal X-ray diffraction. The geometry around the metal center is square-planar. The interaction of two diastereomers of Pd(II) complex with FS-DNA has been explored, using UV-vis spectroscopy, fluorescence quenching, chemometrics and viscosity measurement methods. The **PdL₂¹** exhibited higher binding constant, about 10-fold, ($1.0 \times 10^6 \text{ M}^{-1}$) as compared to **PdL₂²** ($1.5 \times 10^5 \text{ M}^{-1}$). Moreover, the human serum albumin (HSA) binding ability has been monitored by absorption, quenching of tryptophan fluorescence emission and circular dichroism (CD) studies. The slight difference is observed between HSA binding affinity with the complexes: **PdL₂¹** ($6.2 \times 10^4 \text{ M}^{-1}$)

and PdL_2^2 ($3.3 \times 10^4 \text{ M}^{-1}$). Also, the thermodynamic parameters were determined at three different temperatures (298, 308 and 318 K).

In this study, molecular docking was also carried out to confirm and illustrate the specific DNA- and HSA-binding of the Pd(II) complexes. In the PdL_2^1 -HSA system a T-shaped π - π interaction with PHE206 was observed. While in the PdL_2^2 -HSA system there are a hydrogen bond, a π -cation and two T-shaped π - π interactions with ASB324, LYS212 and PHE228, respectively. The groove binding mode of DNA interaction has been proposed for both diastereomers.

Keywords

Pd(II) Schiff base complex

Diastereomers separation

HSA binding

DNA binding

Molecular docking

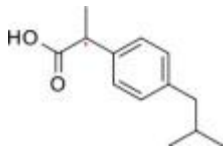
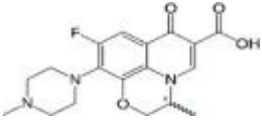
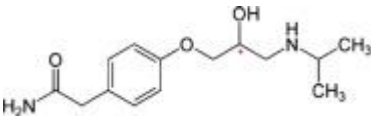
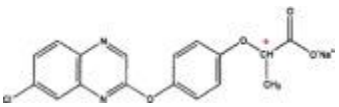
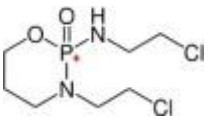
1. Introduction

Cancer, a non-communicable disease, is the major cause of death worldwide [1]. Nowadays, > 100 different kinds of cancer are known. The World Health Organization (WHO) anticipated the increase of cancer deaths from 8.2 million to 13 million annually. Surgery, chemotherapy, radiations and immunotherapy are of the conventional treatments for cancer [2]. Chemotherapy is the mainstay one in which various chemical substances are used. In this way anticancer drugs are circulated throughout the body and reach cancer cells [3]. Platinum-based anticancer drugs including cisplatin, carboplatin and oxaliplatin are potent chemotherapeutic agents that has been clinically used [4]. However, their considerable success is marred due to some drawbacks like drug resistance, normal tissue toxicity and neurotoxicity [4], [5]. The similarity of Pd(II) to Pt(II) analogs, promising biological properties as well as chemotherapeutic potential with different mechanism [6] cause that Pd(II) complexes take attention in this field [7], [8], [9], [10].

The chirality of nucleic acids and the other biomacromolecules such as proteins, enzymes, amino acids, carbohydrates and hormones results in the significance of chirality in pharmaceutical

industries [11]. The introduction of chiral metal complexes as anticancer agent has been started by Lippard et al. in the early 1990s [12]. The emergence of chirality leads to the formation of bioactive compounds with more therapeutic effect due to chirality of most biotargets [13]. Investigation of interaction between chiral metal complexes and biomolecules such as DNA and protein are of current interest in connection with useful information about chiral discrimination of diastereomers and designing bioactive molecules [14]. According to the report of Nguyen et al., 56% of the drugs currently in use are chiral products that 88% of them are racemates consisting of an equimolar mixture of two enantiomers [15]. In Table 1 some commercial drugs that are racemic mixtures are listed.

Table 1. The example of racemic drugs.

Drug	Activity	Structure	Ref
Ibuprofen	Anti-inflammatory, pain medications		[78]
Ofloxacin	Antibacterial		[79]
Atenolol	β -blocker (used in the treatment of hypertension and angina pectoris)		[80]
XK469	Anticancer		[81]
Ifosfamide	Anticancer		[82], [83]

In the current study, we utilized a racemic mixture of Schiff base ligand (**HL**: *R/S*-(1-phenylethylimino)methylnaphtalen-2-ol) to synthesis Pd(II) complex. Aware of the therapeutic activity of naphthalene and 1-phenylethylamine (PEA) [16], [17], [18], [19], [20] these groups were used in the preparation of **HL**. The synthesized complex exists in three different

configurations (Fig. 1A–C). Isomers A and B (homochiral) are non-superimposable mirror images and therefore are enantiomers. Isomer C (heterochiral) have a symmetry center operation and for this reason the complex is not chiral. It is a *meso* form and it is diastereomer of A and B.

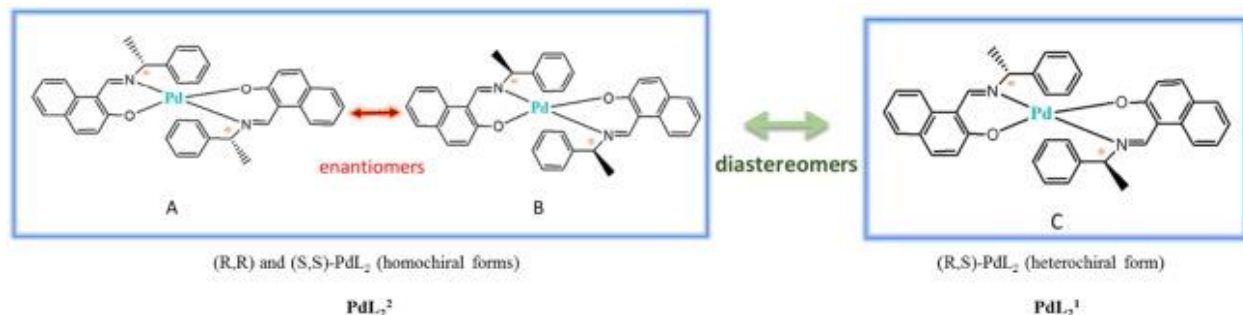


Fig. 1. Four isomers for Pd(II) complex.

We have accomplished separation of these diastereomers into *rac* (*R,R/S,S*-PdL₂) and *meso* (*R,S*-PdL₂) forms by crystallization as a very simple method. Both diastereomers have been characterized by FT-IR, ¹H NMR, ¹³C NMR and elemental analysis. The pure heterochiral (*R,S*) *meso* diastereomer of Pd(II) complex has been synthesized and its structure was determined by single crystal X-ray analysis. Herein, for the first time the biological activities of a heterochiral complex has been assessed. In the current study, the DNA- and HSA-binding of the synthesized complex have been evaluated, using both experimental (fluorescence quenching and UV-vis spectroscopy methods) and computational methods (molecular docking). The circular dichroism spectroscopy has been conducted to study alteration on the secondary structure of HSA causing from HSA-complex interaction. Investigation of thermodynamic parameters at three different temperatures (298, 308 and 318 K) indicates that hydrophobic forces play an important role in the HSA-binding of synthesized complexes. The appearance of fluorescence emission of Pd(II) complexes in the range 550–650 causes that changes of fluorescence of EthBr-DNA was not observed. Hence, Multivariate Curve Resolution Alternating Least Squares (MCR-ALS), a powerful chemometric method, was used to resolve the spectra and concentration profiles of different species involving in equilibrium and to calculate DNA-binding constant of complexes. In addition, the DNA-binding mode of the complexes was investigated using viscosity measurements.

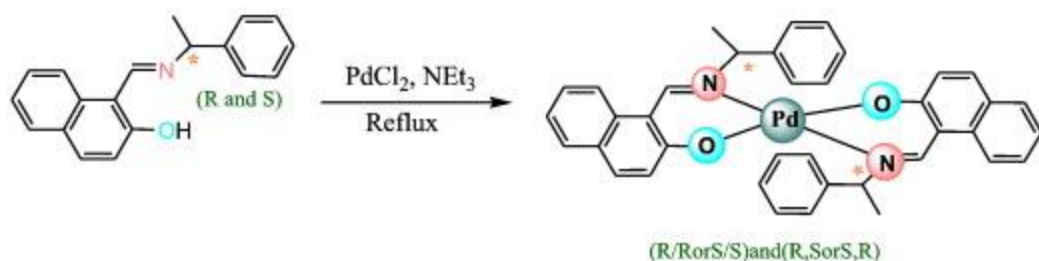
2. Experimental

2.1. Chemicals and Instrumentation

Human serum albumin (HSA), fish sperm DNA (FS-DNA), tris(hydroxymethyl)-aminomethane (Tris), ethidium bromide (3,8-diamino-5-ethyl-6-phenylphenanthridinium bromide, EthBr) were purchased from Sigma-Aldrich. 2-Hydroxy-1-naphthaldehyde and (*R/S*)-1-phenylethylamine were obtained from Merck Co. and used without further purification. All salts used for buffer preparation were analytical grade and were dissolved in double distilled water. All of the solutions were used freshly after preparation. The FT-IR spectrum was recorded on a JASCO, FT/IR-6300 spectrometer ($4000\text{--}400\text{ cm}^{-1}$) in KBr pellets. ^1H and ^{13}C NMR spectra were recorded on a Bruker Avance III 400 spectrometer using CDCl_3 as solvents for palladium(II) complexes. The elemental analysis was performed on Leco, CHNS-932 and Perkin-Elmer 7300 DV elemental analyzers. The UV-vis spectra were recorded on a JASCO V-670 spectrophotometer. Fluorescence measurements were carried out on Shimadzu RF-5000 spectrofluorometer at room temperature. The circular dichroism (CD) spectra were recorded using Aviv spectropolarimeter model 215 (Proterion Corp., USA) at $25\text{ }^\circ\text{C}$. The CD spectra were recorded in the far-UV region ($190\text{--}260\text{ nm}$) using 0.1 cm path length cell and scan speed of 20 nm min^{-1} . MCR-ALS on data was carried out through the MATLAB 7.0 environment (MathWorks Co.) using MCR-ALS 2.0 toolbox (<http://www.mcrals.info/>) [21]. Viscosity was measured using a Brookfield rotational viscometer at room temperature.

2.2. Preparation of Pd(II) Complex

Methanolic solution (10 ml) of 2-hydroxy-1-naphthaldehyde (5 mmol) was added dropwise to a methanolic solution (10 ml) of (*R/S*)-1-phenylethylamine (5 mmol). After continuously stirred for 4 h in ambient temperature, solution of triethylamine (7 mmol) in absolute methanol (5 ml) was added to the solution. The mixture stirred for 30 min , and then a solution of PdCl_2 (2.5 mmol) in absolute methanol (20 ml) was added (Scheme 1).



Scheme 1. Synthesis of Pd(II) complex.

The solution was refluxed overnight to proceed completely. The resulting powder was isolated by filtration. Furthermore, the orange powder was obtained by condensation of filtrate. Both powders were washed by dry methanol several times.

According to ¹H NMR, both resultant precipitates are mixture of *rac* and *meso* diastereoisomers in different ratio (51:49 and 82:18). All products were purified by crystallization from chloroform as a solvent. As a result, two yellow and orange powders were produced. They are Pd-*R,S*-(N[^]O)₂ and Pd-*R,R/S,S*-(N[^]O)₂ which in this paper are named as **PdL₂¹** and **PdL₂²**, respectively. Diffusion of diethyl ether into a DMSO solution of the **PdL₂¹** complex gave orange crystals suitable for crystallography. The typical yield was 61%. Anal. calc. for C₃₈H₃₂PdN₂O₂: C: 69.67, H: 4.92, N: 4.28. Found: C: 69.60, H: 4.86, N: 4.17. Selected IR data (KBr, cm⁻¹): (*R,S* and *S,R*-PdL₂) (**PdL₂¹**): 1612 (νC=N), 1434 (νC=N), 1363 (νC=O) and (*R,R* and *S,S*-PdL₂) (**PdL₂²**):

1610 (νC=N), 1435 (νC=N), 1362 (νC=O). ¹H NMR and ¹³C NMR: Table 2.

Table 2. ¹H and ¹³C NMR of Pd(II) complexes.

	¹ H NMR		¹³ C NMR		
	PdL ₂ ¹	PdL ₂ ²	PdL ₂ ¹	PdL ₂ ²	
OH	—	—	C ₁	164.53	164.54
H ₁	8.36(d)	8.35(d)	C ₂	58.66	58.68
H _{2a}	6.15(q)	6.14(q)	C ₃	21.85	21.87
H _{3a} , H _{3b} , H _{3c}	1.89(m)	1.88(m)	C _{aromatics}	111.43- 155.28	111.41- 155.27
H _{aromatics}	7.10-7.64	7.09-7.65			

s, singlet; d, doublet; t, triplet; m, multiplet

2.3. Single Crystal Diffraction Studies

X-ray data for PdL_2^1 complex was collected on a STOE IPDS-II diffractometer with graphite monochromated Mo-K α radiation. Suitable crystal was chosen using a polarizing microscope and that was mounted on a glass fiber which was used for data collection. Cell constants and an orientation matrix for data collection were obtained by least-squares refinement of diffraction data. Data were collected at a temperature of 298(2) in a series of ω scans in 1° oscillations and integrated using the Stoe X-AREA [22] software package. A numerical absorption correction was applied using the X-RED and X-SHAPE [23] software's. The data were corrected for Lorentz and Polarizing effects.

The structure was solved by direct methods using SIR2004. The non-hydrogen atoms were refined anisotropically by the full matrix least squares method on F^2 using SHELXL [24]. All hydrogen atoms were added at ideal positions and constrained to ride on their parent atoms. Crystallographic data are listed in Table 3. Selected bond distances and angles are summarized in Table 4.

Table 3. Crystal data and structure refinement for PdL_2^1 .

Empirical formula	C₃₈H₃₂N₂O₂Pd
Formula weight	655.06
Temperature (K)	298(2)
Wavelength (Å)	0.71073
Crystal system	Triclinic
Space group	P ₋₁
Unit cell dimensions (Å, °)	a = 8.4415(17)
	b = 9.6060(19)
	c = 9.765(2)

Empirical formula	C₃₈H₃₂N₂O₂Pd
	$\alpha = 83.699(3)$
	$\beta = 83.499(3)$
	$\gamma = 73.282(3)$
Volume (Å³)	751.0(3)
Z	1
Calculated density (Mg/m³)	1.448
Absorption coefficient (mm⁻¹)	0.655
F(000)	336
Theta range for data collection (°)	2.53 to 29.20
Index ranges	$-11 \leq h \leq 7$
	$-13 \leq k \leq 6$
	$-13 \leq l \leq 13$
Reflections collected	4054
Independent reflections	4054 [$R_{\text{int}} = 0.0360$]
Data Completeness (%)	99.4
Refinement method	Full-matrix least-squares on F^2

Empirical formula	C₃₈H₃₂N₂O₂Pd
Data/restraints/parameters	4054/0/197
Goodness-of-fit on F^2	0.956
Final R indices [$I > 2\sigma(I)$]	$R_1 = 0.0442$
	$wR_2 = 0.1116$
R indices (all data)	$R_1 = 0.0477$
	$wR_2 = 0.1145$
Largest diff. peak and hole ($e \cdot \text{\AA}^{-3}$)	0.658 and -1.337

Table 4. Selected bond distances (\AA) and angles ($^\circ$) for **PdL**^{1,2}.^a

Pd(1)–O(1)	1.982(2)	N(1)–C(11)–C(10)	128.9(3)
Pd(1)–N(1)	2.017(2)	N(1)–C(12)–C(19)	109.9(3)
N(1)–C(7)	1.298(4)	N(1)–C(12)–C(13)	110.5(2)
O(1)–C(1)	1.310(4)	Pd(1)–N(1)–C(12)–C(13)	120.6(2)
		C(11)–N(1)–C(12)–C(19)	68.0(3)
O(1)–Pd(1)–O(1')	180.00(14)	C(12)–N(1)–C(11)–C(10)	$-174.9(3)$
O(1)–Pd(1)–N(1)	89.24(9)	Pd(1)–N(1)–C(12)–C(19)	$-110.3(2)$
O(1)–Pd(1)–N(1')	90.76(9)	Pd(1)–N(1)–C(11)–C(10)	3.39(2)
N(1)–Pd(1)–N(1')	180.00(16)	C(11)–N(1)–C(12)–C(13)	$-61.06(2)$

Pd(1)–O(1)	1.982(2)	N(1)–C(11)–C(10)	128.9(3)
C(1)–O(1)–Pd(1)	116.2(2)	N(1)–Pd(1)–O(1)–C(1)	18.5(2)
C(11)–N(1)–Pd(1)	123.28(19)	O(1)–Pd(1)–N(1)–C(12)	165.2(2)
C(12)–N(1)–Pd(1)	120.50(18)		

a

Symmetry transformations used to generate equivalent atoms: 1-x,-y,-z.

2.4. DNA Binding Studies

The stock solution of FS-DNA was prepared in 50 mM Tris buffer at pH 7.5 using double-distilled deionized water and stored at 4 °C. The FS-DNA concentration per nucleotide was determined by the absorption intensity at 260 nm after adequate dilution with the buffer and using the reported molar absorptivity of $6600 \text{ M}^{-1} \text{ cm}^{-1}$. Purity of FS-DNA solution was confirmed by ratio of UV absorbance at 260 and 280 nm ($A_{260} / A_{280} = 1.9$), indicating that FS-DNA is free from protein impurity [25]. The solution of the compounds was first prepared in DMF, and then diluted with corresponding buffer to required concentration for all experiments. The volume of DMF never exceeded 0.3% (v/v), so the effect of DMF is negligible. The UV–vis spectral features of the complexes did not change on keeping its buffered or DMF solution for 24 h and no precipitation or turbidity was observed even after long storage at room temperature, which indicates the stability of the complexes in different media. However, all the solutions were used freshly after preparation.

The binding character of the Pd(II) complexes toward FS-DNA has been investigated by UV–vis spectroscopy. Spectrophotometric titration experiments were performed by addition of various amounts of DNA ($1.5 \times 10^{-4} \text{ M}$) to the Pd(II) complexes ($2 \times 10^{-5} \text{ M}$). At each titration step, the mixture solutions were allowed to incubate for 2 min before recording the related spectra. In addition, the equal amount of DNA solution was added to the blank solution to eliminate its absorbance.

The DNA-binding constant of the Pd(II) complexes was also determined by analyzing the fluorescence data obtained from titration of DNA-EthBr with the Pd(II) complexes using MCR-

ALS method. To this aim, a mixture solution of FS-DNA and EthBr at molar ratio of 10:1 was stirred for 1 h at 4 °C. Then, various amounts of Pd(II) complexes were added to this mixture. The fluorescence spectra upon the titration were recorded in the range of 550–700 nm with exciting wavelength at 520 nm. The fluorescence quenching experiment was carried out using quartz cuvette with 1 cm optical path length and the excitation and emission slits set at 5 and 10 nm, respectively. In each measurement, the complex–DNA solutions were allowed to incubate for 2 min before recording. Due to spectra overlapping of Pd(II) complexes and DNA-EthBr, the study of their interaction based on fluorescence data is not straightforward. Therefore, the MCR-ALS method has been utilized to resolve spectra as well as the concentration profiles of all species in solution.

Viscosity experiments were carried out using a rotational viscometer and the measurements were performed at 200 rpm at room temperature. The viscosity of DNA solution was measured in the presence of increasing amounts of the Pd(II) complexes. The obtained data are presented as $(\eta/\eta^0)^{1/3}$ versus [complex]/[DNA], where η and η^0 are the viscosity of DNA in the absence and presence of the compounds, respectively.

2.5. HSA Binding Experiment

A stock solution of HSA was prepared by dissolving the desired amount of HSA in 50 mM phosphate buffer (pH = 7). The HSA stock solution was stored at 4 °C in the dark and used within 2 h. Its concentration was determined by UV–vis spectrophotometry using the molar absorption coefficient $35,700 \text{ M}^{-1} \text{ cm}^{-1}$ at 278 nm [26].

Absorption titration experiment, an operational and very easy method, was carried out to investigate the HSA-binding of complexes at room temperature. The UV–vis absorption spectra of the HSA solution ($5 \times 10^{-6} \text{ M}$) in the absence and presence of various amounts of Pd(II) complexes ($0\text{--}25 \times 10^{-6} \text{ M}$) were recorded after 2 min incubation.

The interaction of HSA with the synthesized Pd(II) complexes was investigated using fluorescence quenching experiment. In this experiment 2 ml of HSA solution ($3 \times 10^{-6} \text{ M}$) was placed into the cell while various amounts of Pd(II) complexes ($0\text{--}25 \times 10^{-6} \text{ M}$) were added to the cell at room temperature. The fluorescence intensity was measured with excitation wavelength at 295 nm and emission wavelength rang of 300–450 nm. In each measurement the mixture was allowed to

incubate for 2 min after addition of the complexes. The fluorescence emission spectra were recorded at three different temperatures (298, 308, and 318 K).

The absorptions of HSA at the excitation and emission wavelengths is approximately zero in all concentrations. Hence, a reduction in the emission intensity is independent of the inner filter effect. Furthermore, all intensities were corrected for the dilution effect in fluorescence and UV absorption experiments for DNA- and HSA-binding.

Furthermore, the circular dichroism (CD) spectrum was recorded at room temperature in the range of 190–260 nm, using 0.1 cm quartz cell. The CD spectrum of HSA solution was recorded before and after addition of the synthesized complexes with molar ratio 0, 0.5, 1 and 2. This analysis was carried out by CDNN software. The content of secondary conformation of HSA in each step was calculated from this technique. The spectra were obtained by subtracting the spectra of the complexes as baseline.

2.6. Molecular Docking Simulation

In this work, docking study was carried out to indicate the DNA and HSA-binding site for the synthesized complexes. The 3D structures of (*R,S*)-**PdL₂** complex was generated using the CIF files of its X-ray crystal structures. The CIF files were converted to the PDB format by using the Mercury software (<http://www.ccdc.cam.ac.uk/>). The optimized structure of (*R,R/S,S*)-**PdL₂** complex was calculated using Gaussian 09 [27] at the levels of B3LYP/LANL2DZ and B3LYP/6-31G** for Pd and the other atoms, respectively. The known crystal structure of DNA (PDB ID: 423D) with sequence d(ACCGACGTCGGT)₂ and HSA (PDB ID: 1AO6) were taken from the Brookhaven Protein Data Bank (<http://www.rcsb.org/pdb>) at resolution of 1.60 and 0.25 Å, respectively. Water molecules of the .pdb files were removed, missing hydrogen atoms and Gasteiger charges were added. Flexible-ligand docking was performed by AutoDock 4.2 molecular-docking program using the implemented empirical free energy function and the Lamarckian Genetic Algorithm [28]. The Gasteiger charges were added to prepare the macromolecule input file for docking and the Auto Grid was used to calculate Grids. A blind docking with 126 lattice points along X, Y, and Z axes was performed to find the active site of ligands to the biomacromolecules. After determination of the active site, the dimensions of the grid map were selected 60 points with a grid point spacing of 0.375 Å, to allow the ligand to rotate freely. 200 docking runs with 25,000,000 energy evaluations for each run were performed.

3. Result and Discussion

3.1. IR Spectra

Characteristic IR bands and their assignments are given in Section 2. In the FT-IR spectra of the complexes the absence of the phenolic O-H vibration is indicative of deprotonation of ligand to coordination through oxygen atoms. The stretching band of the imine group (C=N) appeared at 1612 and 1610 cm^{-1} for **PdL₂¹** and **PdL₂²** complexes, respectively [26]. The strong bands related to the C=O and C=N stretching were observed at the region of 1363 and 1434 cm^{-1} for **PdL₂¹**, 1362 and 1435 cm^{-1} for **PdL₂²** complexes. The presence of several medium intensity bands between 2800 and 3100 cm^{-1} in the spectra of Pd(II) complexes suggests the existence of C-H stretching vibrations of aliphatic and aromatic protons.

3.2. NMR Spectra

In this study, nuclear magnetic resonance (NMR) was utilized to study separation of two diastereomers (racemic and *meso* forms). The reliable results are obtained by this technique without use of molecular interactions with reagents, chromatography columns and etc. [29]. There are some literatures in which the diastereomeric ratio was obtained using NMR by the integration of characteristic signals with different chemical shifts for diastereomers [29], [30]. The appearance of two signals for imine proton (H-C=N) in ¹H NMR of resultant precipitate and filtrate indicates the existence of two diastereomers in each solution (Fig. 2), as previously reported [30], [31].

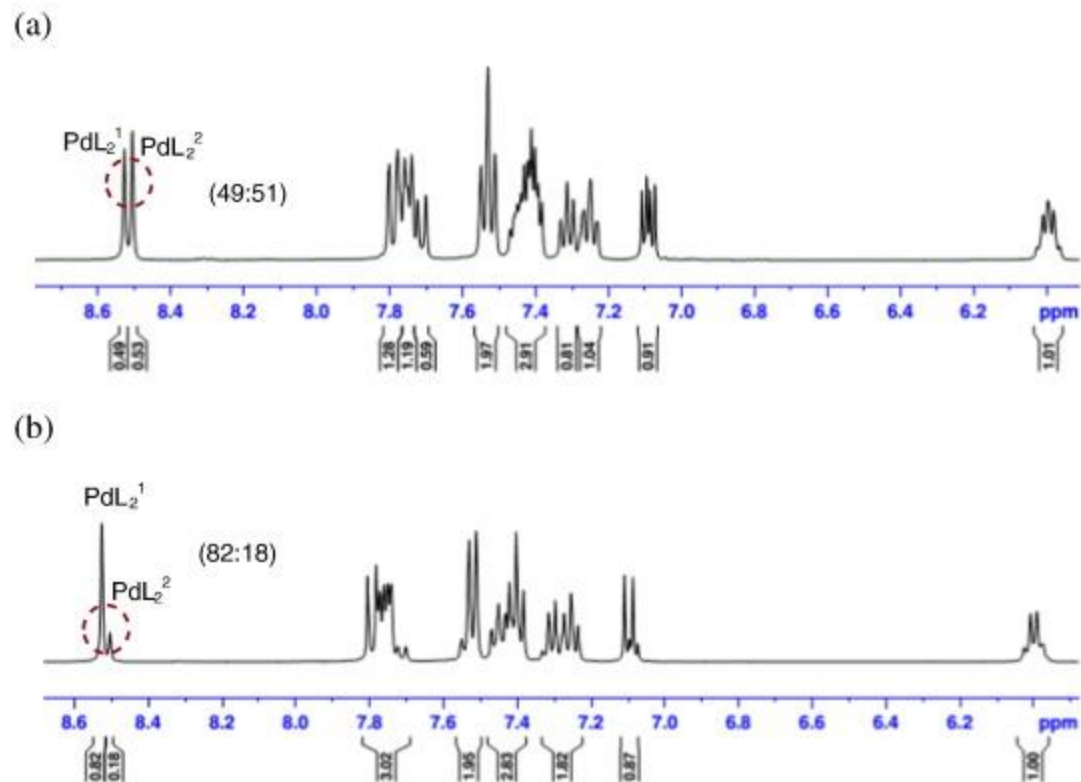


Fig. 2. ^1H NMR spectra of mixture of diastereomers in (a) precipitate and (b) filtrate in preparation of Pd(II) complex, the ratio of two diastereomers is shown (See Section 2).

There are two diastereomers (PdL_2^1 and PdL_2^2) in both solution with different molar ratio. Separation of the diastereomers by crystallization in several solvents was tested, finally it was successful with chloroform which suggests different solubility properties of isomers. Complexes PdL_2^1 and PdL_2^2 have similar ^1H NMR spectra in CDCl_3 (Fig. 3).

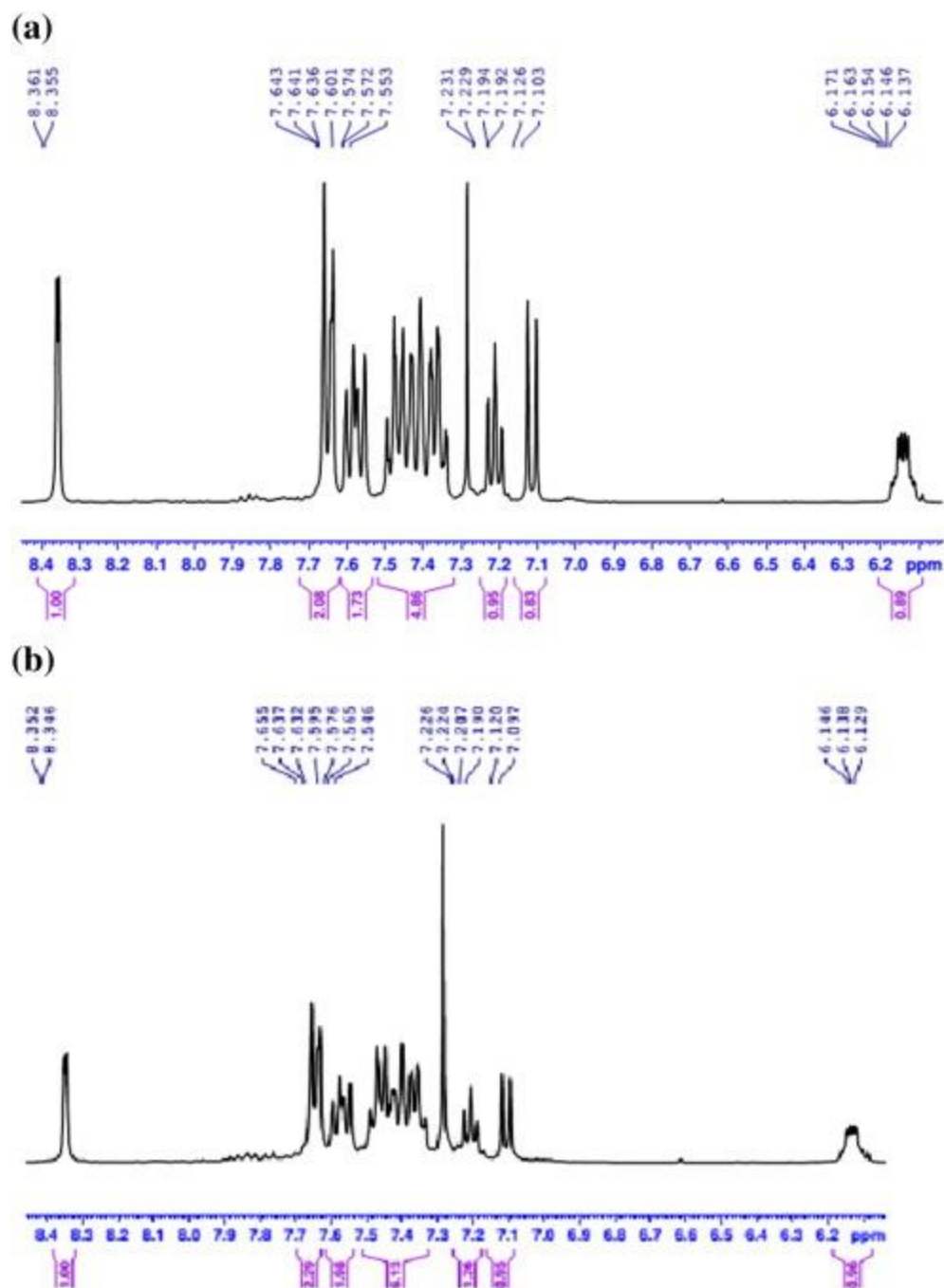


Fig. 3. The ^1H NMR spectra of two diastereomers of Pd(II) complex.

The single signal for imine proton in ^1H NMR confirmed the successful separation of diastereomers. This signal is doublet that can be attributed to coupling between H_1 and H_4 (Fig. 4).

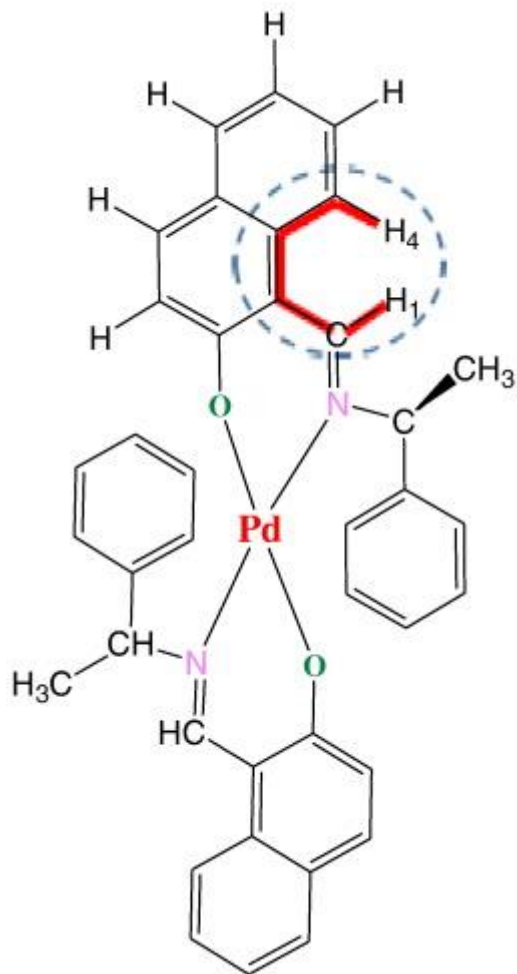


Fig. 4. Long-range coupling of H₁ and H₄.

The Pd(II) complexes are rigid and therefore the imine hydrogen is located close to H₄ and the long-range coupling is observed. In Pd(II) complexes the value of 5J of H₁ and H₄ is equal to 2.4 Hz that is close to the reported value (in the range of 0–2 Hz) [32]. As expected, the NMR spectra of the diastereomeric complexes (**PdL₂¹** and **PdL₂²**) exhibited different stereochemistry at the imine and CH which shows little differences in the chemical shift. The related signals of ¹H and ¹³C NMR experiments were listed in Table 2. The resonance signal due to phenolic OH proton disappears in the Pd(II) complexes, indicating the coordination of oxygen atom to Pd(II) ion. A characteristics feature of the ¹H NMR spectra of **PdL₂¹** and **PdL₂²** is the imine proton resonance at 8.36 and 8.35 ppm, respectively, along with the signal (q, 1H) assigned to the

CH proton which appears at 6.15 and 6.14 ppm and the signal (d of d, 3H) at 1.89 and 1.88 ppm which is due to CH_3 of PdL_2^1 and PdL_2^2 , respectively. The splitting is in view of coupling hydrogen of CH_3 with CH and HC N hydrogens.

The ^{13}C NMR spectra of PdL_2 complexes show 19 signals. The peaks observed at 164.54 and 164.53 ppm is ascribed to the imine carbon atoms of PdL_2^1 and PdL_2^2 , respectively. The existence this band in the spectra of complexes supports the presence of the Schiff base in the complex.

The ^1H and ^{13}C NMR were run immediately after dissolving complexes in chloroform and gave the expected simple spectra, indicating the integrity of the complexes. No epimerization was observed when the solutions left to stand and their NMR spectra were similar to the initial one.

3.3. Description of the Crystal Structure of PdL_2^1

An ORTEP view of PdL_2^1 (*R,S-PdL*₂) with the atom-numbering scheme is presented in Fig. 5 and the crystallographic data and selected bond lengths and angles are collected in Table 3, Table 4. In the solid state, PdL_2^1 has a crystallographic center of symmetry that is right in the middle point of the palladium(II) ion in a planar-transoid conformation (Fig. 5). The molecular unit is centrosymmetric and is made up of equivalent halves. The 1-phenylethylamine groups show a fixed conformation in the crystal packing.

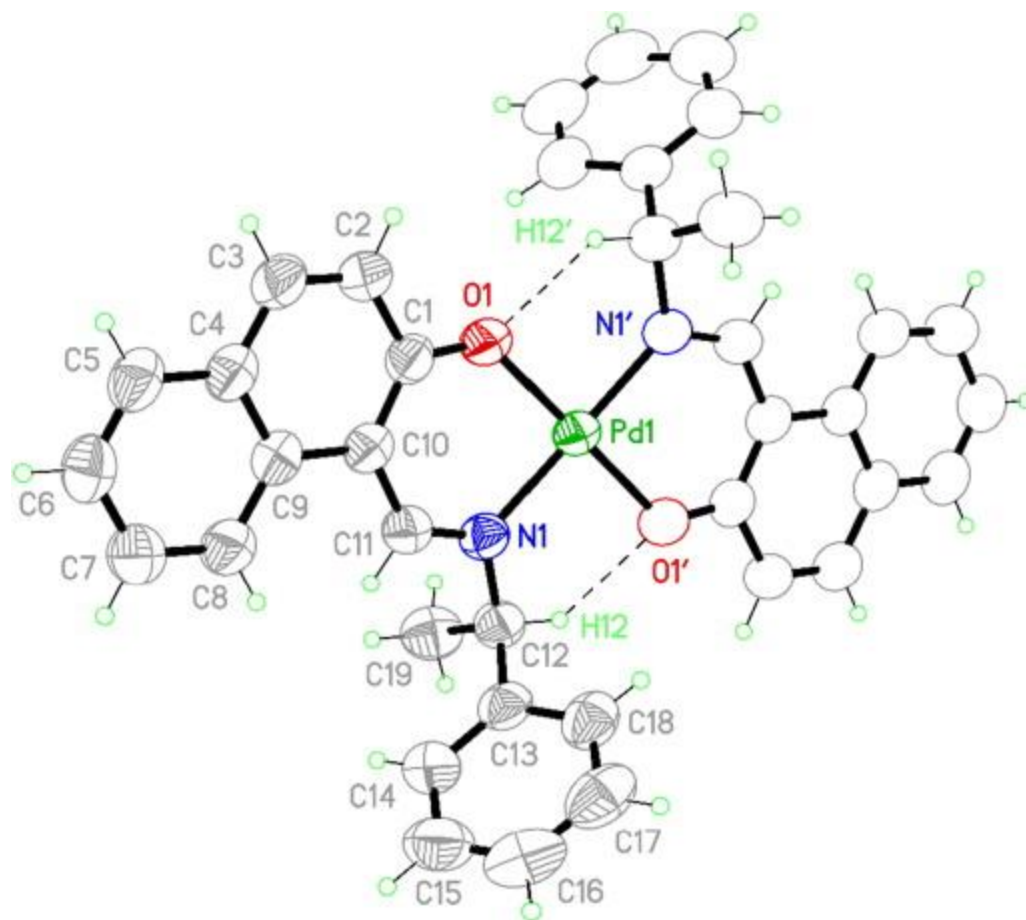
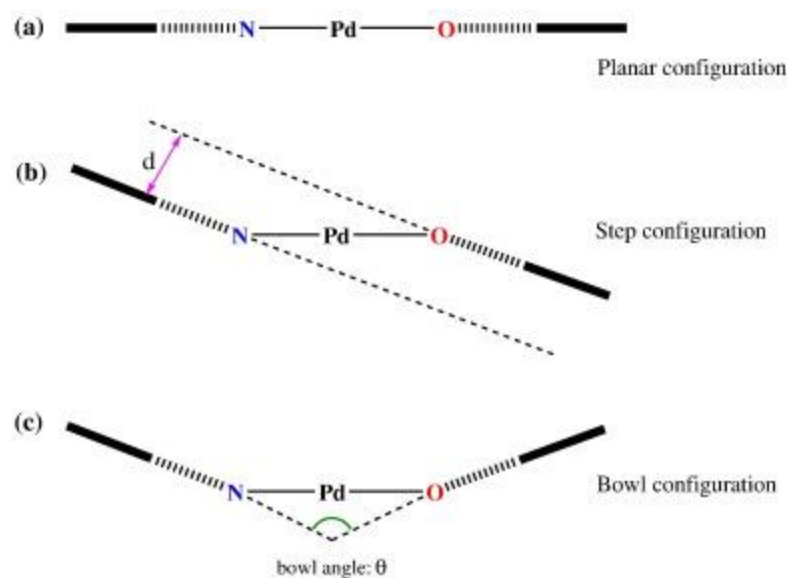


Fig. 5. ORTEP representation of PdL_2 . Displacement ellipsoids are drawn at the 50% probability level and H atoms are shown as small spheres of arbitrary radii. Hydrogen bonds are shown as dashed lines.

Single crystal X-ray structure determination for PdL_2^1 shows that two Schiff base ligands with different chirality (*R*-(1-phenylethylimino)methylnaphtalen-2-ol and *S*-(1-phenylethylimino)methylnaphtalen-2-ol) ligands coordinate to the palladium atom with their imino-nitrogen and phenoxide-oxygen atoms. The crystallographic data reveal that the two monoanionic *N,O*-bidentate Schiff base ligands form a slightly distorted square planer around the Palladium atom. As can be seen in Table 4, the bond angles O(1)–Pd(1)–N(1) [89.24(9)] and O(1)–Pd(1)–N(1') [90.76(9)°] are close to 90°. The two nitrogen atoms (and subsequently the two oxygen atoms) are *trans* positioned such that two phenyl substituents lies both sides of the $[\text{MO}_2\text{N}_2]$ plane. The Pd–O distance [Pd(1)–O(1) = 1.982(2) Å] and the Pd–N bond length

[Pd(1)–N(1) = 2.017(2) Å] are as expected from literature reports for similar Pd(II) complexes [33], [34]. For instance, distances of 1.987(3) Å for Pd–O bond and 2.066(3) Å for Pd–N bond are found in a related di-(2-allyliminomethylphenolato)palladium(II) complex derived from allylamine and salicylaldehyde [34]. The C–N bond distances are 1.288(9) Å (N1 = C11) and 1.325(8) Å (N2 = C25), which is consistent with a slight elongation of the C–N double bond when coordinates to a metal center [35].

The *trans*-Pd(N,O)₂ complexes can subdivide into three classes (Scheme 2): planar configuration (with the distance between mean planes of the aromatic rings less than $d = 0.4$ Å) (See for example Refs. [36], [37].), step configuration (with the distance between mean planes of the aromatic rings greater than $d = 0.4$ Å) (See for example Refs. [38].), bowl configuration (See for example Refs. [39], [40].).



Scheme 2. Planar, step and bowl configurations in bis(salicylideneimine)palladium(II) complexes. —square of Pd, O, and N atoms; —||||| chelate rings; — arene rings.

In the complexes Pd(N,O)₂ with planar configuration the Pd atom lies in the plane of the chelate rings (See for example Refs. [36], [37].). The two six-membered chelate rings and their annulated phenyl rings are coplanar (Scheme 2a). The complexes have inversion symmetry. Frequently, a

characteristic feature of Pd(N,O)₂ complexes is an envelope configuration of the six-membered chelate rings with the Pd atom deviating from the plane of the other 5 atoms of the chelate rings. The direct consequence is the alternative of a step or a bowl configuration (Scheme 2b and c). In the step configuration the planes between the aromatic rings are parallel to each other (See for example Refs. [38].) and the complexes still have C_i symmetry. Some Pd(II) complexes adopt a bowl configuration (See for example Refs. [39], [40].), and have C₂ symmetry. According to the above description, the **PdL₂** complex has planar configuration.

As shown in Fig. 5, there are two intramolecular nonclassical C—H...O hydrogen bonds in **PdL₂**¹. Intramolecular hydrogen bond occurs between C(12)—H(12)...O(1)' atoms and C(12)'—H(12)'\dots O(1) [2.137(2) Å] atoms (Fig. 5).

3.4. Interaction with DNA

3.4.1. UV-Vis Absorption

Electronic absorption spectroscopy is an effective method to receive valuable information about binding mode and binding affinity of metal complex to DNA [25]. Generally, hyperchromic or hypochromic effect and red or blue shift are observed in the UV-vis spectrum of a drug upon its DNA-binding. Hypochromic and red shift is indicative of intercalation mode involving an interaction between π*-orbital of drug with π-orbital of DNA base pairs [41]. Therefore, energy level of π*-orbital of drug decreases which causes red shift in its UV-vis spectrum. Furthermore, the coupled π*-orbital is filled and so the probability of electron transition decreased and hypochromic is observed [41], [42]. While a groove binding or electrostatic interaction leads to hyperchromic effect along with blue shift [43]. A hyperchromic effect can be due to breakage of the secondary structure of DNA [44], [45].

The absorption spectra of the complexes in the absence and presence of different concentrations of FS-DNA were given in Fig. 6.

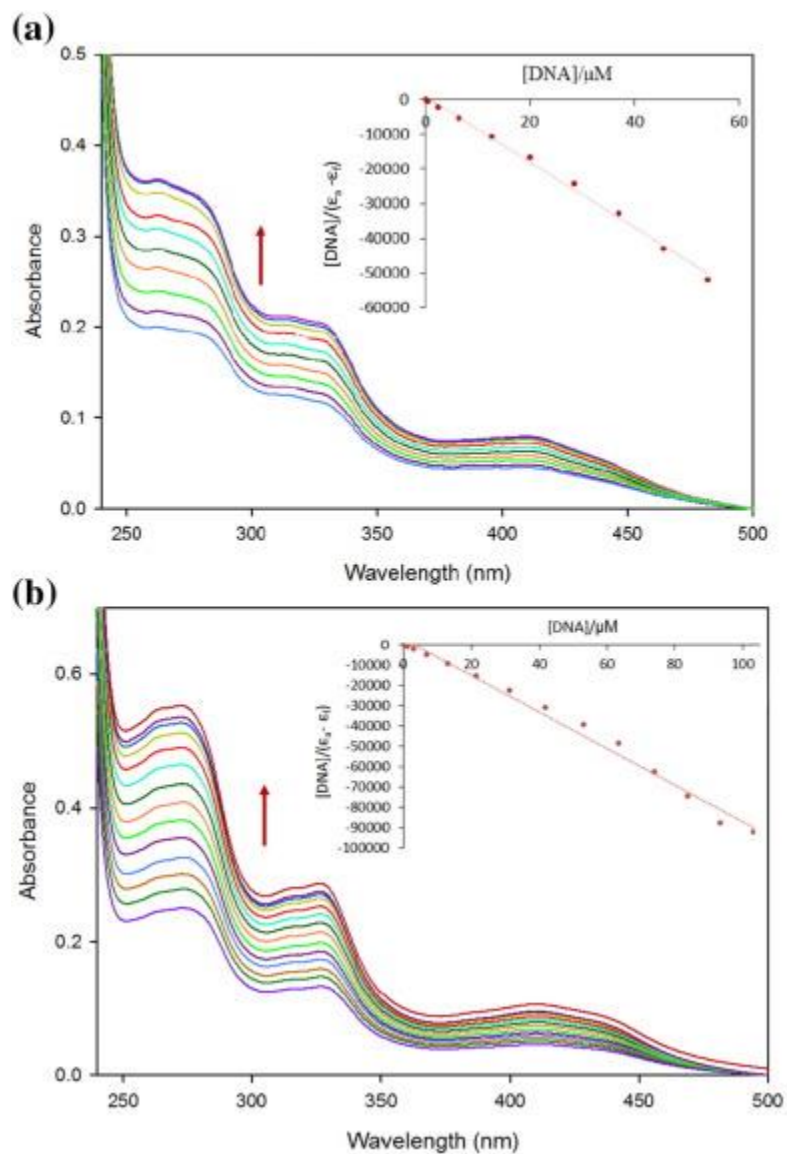


Fig. 6. The change of electronic absorption spectra of a) **PdL₂¹** and b) **PdL₂²** complexes (2×10^{-5} M) upon addition various amounts of FS-DNA (1.5×10^{-4} M).

As shown in this figure, the absorption spectra of the Pd(II) complexes mainly consist of three absorption bands at 272, 326 and 410 nm for **PdL₂¹** and 262, 329 and 409 for **PdL₂²**. The bands below 330 nm are attributed to π - π^* and n- π^* transitions of the ligands. The absorption bands appear at 410 and 409 nm ascribed to the metal to ligand charge transfer transitions [46], [47]. The intensity of these peaks increased with the addition of FS-DNA. These spectral characteristics suggest that the complexes can interact through groove binding mode [48].

To quantitatively evaluate the affinity of compounds with FS-DNA, the intrinsic binding constant K_b was determined by monitoring the changes in absorbance using the following equation [48]:

$$\frac{[\text{DNA}]}{\varepsilon_a - \varepsilon_f} = \frac{[\text{DNA}]}{\varepsilon_b - \varepsilon_f} + \frac{1}{K_b(\varepsilon_b - \varepsilon_f)} \quad (1)$$

Where [DNA] is the concentration of FS-DNA; ε_a , ε_f and ε_b are the apparent extinction coefficient, the extinction coefficient for free compounds and the extinction coefficient for the compounds in fully bound form, respectively. ε_f was determined by calibration curve and ε_a is the ratio of A_{obs} to [compound]. A plot of $[\text{DNA}] / (\varepsilon_a - \varepsilon_f)$ versus [DNA] gives K_b as ratio of slope to y-intercept. The binding constant of FS-DNA with **PdL₂¹** and **PdL₂²** are determined as 1.0×10^6 and $1.5 \times 10^5 \text{ M}^{-1}$, respectively.

3.4.2. MCR-ALS Method

The MCR-ALS is a powerful chemometrics method usually used to resolve of multicomponent mixtures into a simplified model. This methodology decomposes the multicomponent experimental data matrix to evaluate concentration profiles and pure spectra of chemical components simultaneously present in the system [49], [50]. The detailed steps for the MCR-ALS procedure have been previously described [21] in which the decomposition of the experimental data matrix (D) was performed according to the following equation:

$$D = CS^T + E \quad (2)$$

Where D (n, m) is the experimental bilinear data matrix, n denotes for the number of the recorded spectra (i.e. the number of titration step) and m gives the number of wavelengths measured in every spectrum. C (n, q) is the matrix which contains the concentration profiles of the q spectroscopically active species. Matrix S^T (q, m) is the spectroscopic matrix consisting of the pure emission spectra. E (n, m) is the residual matrix with data variation not explained by the proposed contributions [51]. The use of MCR-ALS includes the following steps: (i) experimental data arrangement in matrix D(n × m); (ii) determination of number of chemical species; (iii) initial

estimate of the concentration profiles and pure spectra. (iv) applying different constraints (such as non-negativity, unimodality, closure, ...) to model [52].

We utilized the MCR-ALS to analyze obtained fluorescence data from titration of DNA-EthBr with Pd(II) complexes. Ethidium bromide (EthBr) is a standard intercalating agent of DNA that is used to study DNA-binding of compounds. It was known that EthBr has only a weak fluorescence emission in solution, while a significant increase of its fluorescence intensity can be observed when it binds to DNA in view of its strong intercalation between the adjacent base pairs of DNA [53]. In our study, due to fluorescence emission of Pd(II) complexes in the range 550–650 quenching is not clearly observed. Fig. 7 shows the experimental fluorescence emission of pure solutions of Pd(II) complexes (100 μM) and DNA-EthBr (50: 5 μM).

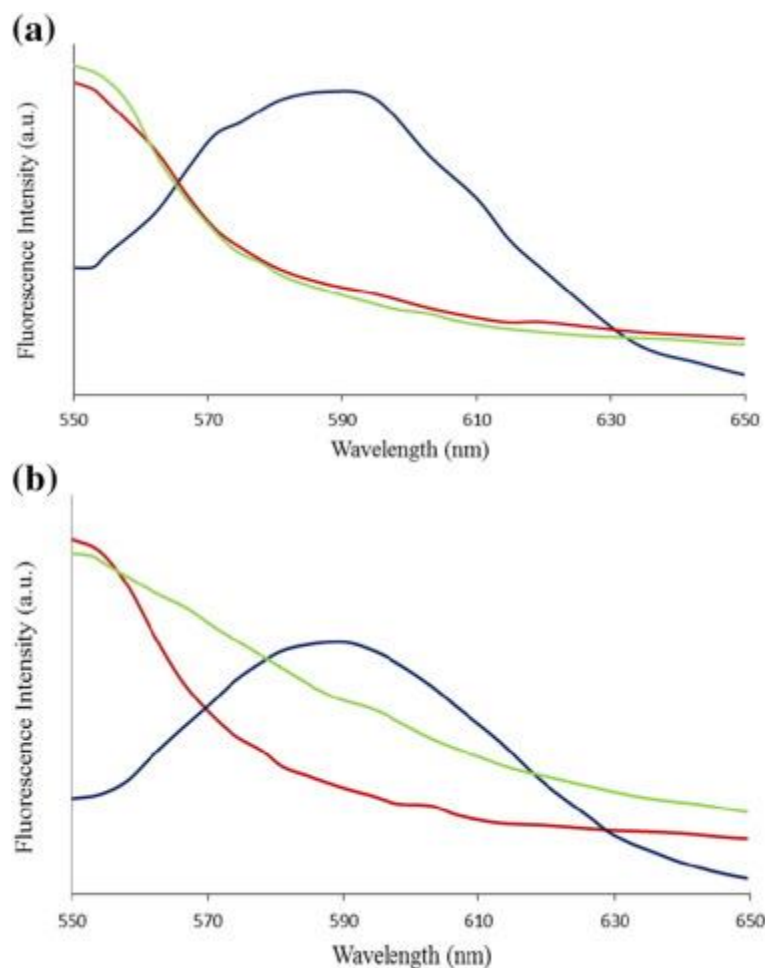


Fig. 7. (a) The fluorescence spectra and (b) spectra profile of **PdL₂¹**, **PdL₂²** and DNA-EthBr.

As it is obvious, the fluorescence spectra of mentioned compounds are highly overlapped. Hence, MCR-ALS method was performed to decompose fluorescence data to spectra and concentration profiles [54]. By applying some constrain to MCR-ALS method (i.e. closure, no negativity and unimodality) for both spectra and concentration, the experimental fluorescence data decomposed to spectra and concentration profiles. The Fig. 7 shows the resolved spectra profiles for DNA-EthBr and Pd(II) complexes. As can be seen, the resolved spectra profiles are very closed to those recorded for pure components (Fig. 7). This indicates the ability of MCR-ALS in resolving of pure spectra profiles from experimental data. Finally, from the concentration profiles, the binding constant of DNA with **PdL₂¹** and **PdL₂²** were calculated as 2.3×10^5 and $4.9 \times 10^4 \text{ M}^{-1}$ respectively.

The results obtained from the above experiments suggested that both **PdL₂¹** and **PdL₂²** complexes can strongly bind to FS-DNA and are comparable to obtained data for the other Pd(II) complexes. For instance, $7.9 \times 10^5 \text{ M}^{-1}$ for [Pd(DeaSal-tsc)(PPh₃)] [46], $1.7 \times 10^5 \text{ M}^{-1}$ for [Pd(H-Msal-tsc)(PPh₃)] [55] and $5.8 \times 10^4 \text{ M}^{-1}$ [Pd(Nap-tsc)(AsPh₃)] [8].

3.4.3. Viscosity Measurement

To further verify the interaction mode of the Pd(II) complexes with DNA, viscosity measurements of DNA upon addition of the complexes were carried out. A classical intercalative mode causes an increase in the DNA viscosity. Because base pairs are separated in order to accommodate the binding ligand and then the overall length of DNA increases [17], [38]. Non-classical mode of interactions such as groove binding and electrostatic could bend the DNA helix, reduces its length and causes the reduction or no change in the DNA viscosity [39]. The effect of the Pd(II) complexes on the viscosity of DNA is illustrated in Fig. 8 As can be seen, the viscosity of DNA decreased slightly with an increasing amounts of the complex, indicating the binding mode of both complexes may be groove binding.

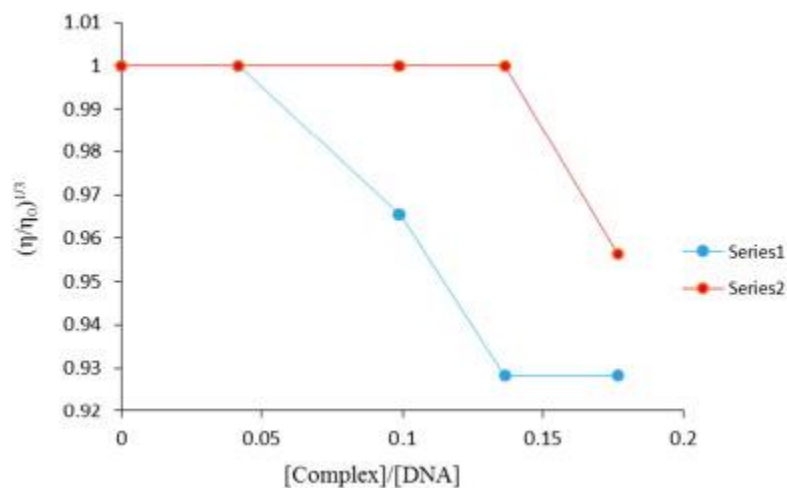


Fig. 8. Effect of increasing amounts of Pd(II) complexes on the viscosity of DNA. $[\text{complex}] / [\text{DNA}] = 0, 0.05, 0.1, 0.15, 0.2, 0.3$.

The degree of reduction of DNA viscosity, which may depend on affinity of Pd(II) complexes to DNA, follows the order of $\text{PdL}_2^1 > \text{PdL}_2^2$, which is inconsistent with UV-vis and fluorescence spectroscopy results.

3.4.4. Docking Study

Molecular docking studies were carried out to obtain a theoretical insight into the DNA binding of Pd(II) complexes. The docked model results suggest that both complexes bind with the minor groove of DNA (Fig. 9).

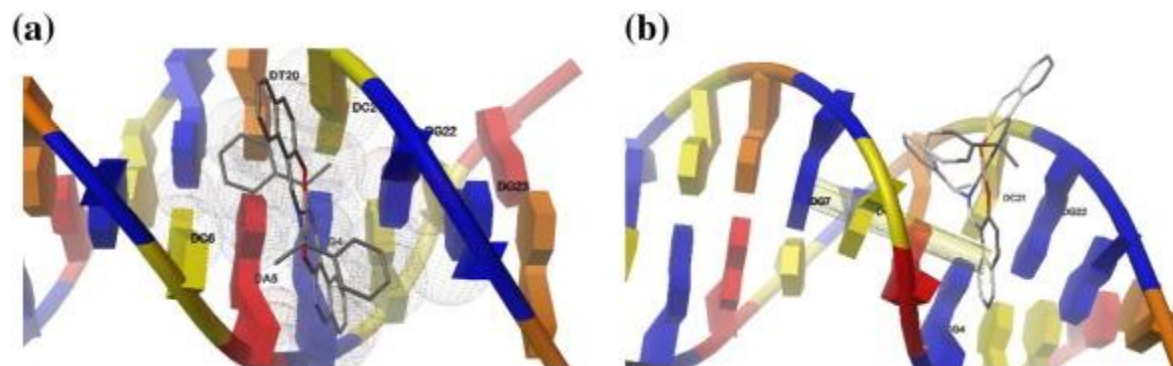


Fig. 9. Presentation of the interaction of a) PdL_2^1 and b) PdL_2^2 complexes with the minor groove of DNA.

The **PdL₂¹** interacts with DG23, DG22, DC21, DT20, DC6, DA5 and DG4 nucleotides. While the interaction of the **PdL₂²** with DC6, DG7, DA5, DG4, DC21 and DG22 nucleotides has been observed. This complex formed two π - π interactions with DG7 nucleotide. The binding free energies (ΔG), describing the affinity of the complexes binding to DNA with the best scores, are -7.7 and -7.47 kcal mol⁻¹ for **PdL₂¹** and **PdL₂²**, respectively. These results revealed the stronger DNA-binding of **PdL₂¹** with a slight difference. Both the experimental results and computational docking data collectively suggest that the synthesized complexes are DNA groove binder.

3.5. Interaction with Human Serum Albumin (HSA)

3.5.1. UV-Vis Absorption

Interaction between a drug and protein affects on drug absorption, distribution and elimination in the circulatory system [56]. Moreover, this binding can prevent rapid elimination of drugs from bloodstream [57], and also increase drug solubility in plasma, decrease its toxicity, protect from oxidation and prolong its in vivo half-life [58]. The exigency of HSA-binding study in synthesis and design new drugs motivated us to investigate HSA-binding behaviour of Pd(II) complexes. Consequently, fluorescence quenching experiment has been carried out to obtain information including binding mode, binding constants, number of binding sites and intermolecular distances [59]. The UV-vis absorption spectroscopy has been also performed to calculate binding constant. More detailed about conformational changes of secondary structure of HSA has been detected by means of CD spectroscopy.

UV-vis absorption spectroscopy is an effective and simple technique to study the HSA-drug binding and to investigate structural changes of protein upon its drug binding. The UV absorption spectra of HSA shows a strong absorption peak at about 220 nm resulted of the $n \rightarrow \pi^*$ transition for the peptide bond of α -helix and a weak peak at 278 nm assigned to $\pi \rightarrow \pi^*$ transition of the phenyl rings in aromatic acid residues (Trp, Tyr and Phe) [60]. Through addition of various amount of the prepared complexes (5×10^{-5} M), the absorption peak at 287 nm for free HSA increases (hyperchromic) (Fig. 10), indicating the interactions between HSA and the complexes. Moreover, observation of hyperchromic effect in UV-vis spectra of HSA reveals the change of environment of the Tryptophan (Trp-214) residue, and the slight increase in hydrophobicity of the microenvironment of the Trp-214 residue [61].

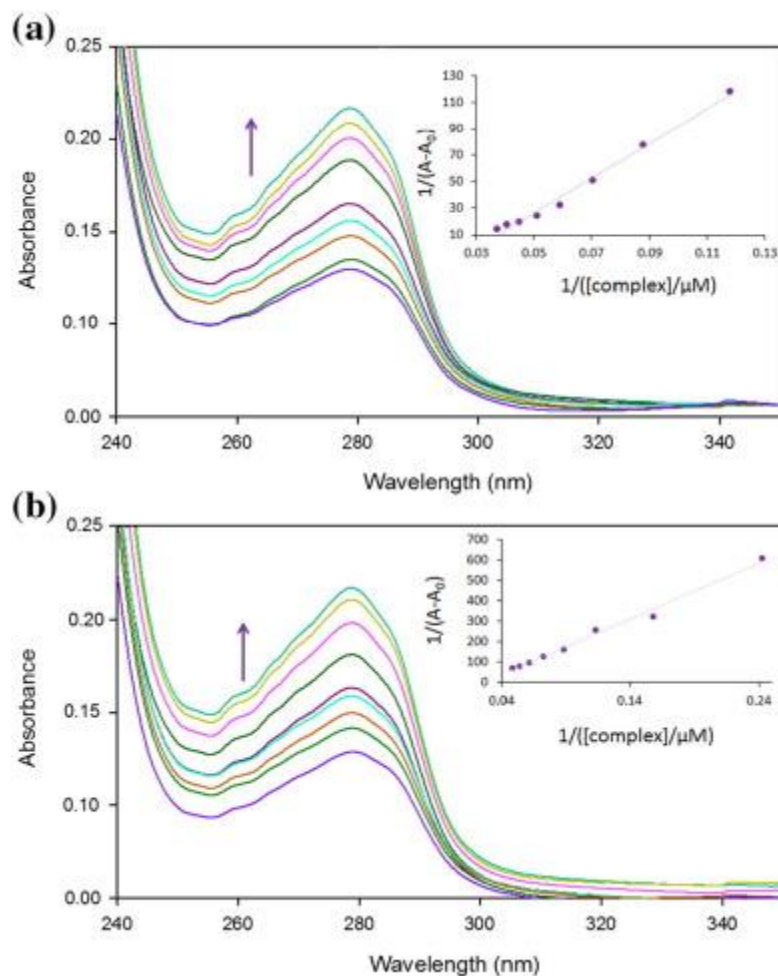


Fig. 10. The change of electronic absorption spectra of HSA (5×10^{-6} M) upon addition various amounts of a) **PdL₂¹** and b) **PdL₂²** (5×10^{-5} M).

In order to assess the binding ability of the title complexes with HSA, the intrinsic binding constant (K_b) was determined by monitoring the changes of absorbance with increasing concentration of the compounds and using Benesi–Hildebrand plot and the following equation [62], [63]:

$$\frac{1}{(A-A_0)} = \frac{1}{(A_{max}-A)} + \frac{1}{K_b(A_{max}-A)} \times \frac{1}{[M]} \quad (3)$$

Where A_0 and A are the absorbance of HSA in the absence and presence of drug, respectively. A_{max} is the obtained absorbance at saturation and $[M]$ is the concentration of complex [63]. The plot of $1/(A - A_0)$ versus $1/[M]$ gives K_b as ratio of y-intercept to slop. The binding constants for **PdL₂¹** and **PdL₂²** are equal to 3.5×10^4 and 2.9×10^4 M⁻¹, respectively (Fig. 10).

3.5.2. Fluorescence Spectroscopy

Fluorescence quenching experiment has been performed to investigate the mechanism of interaction between HSA and the compounds. Although the fluorescence of HSA arises from tryptophan (Trp), tyrosine (Tyr), and phenylalanine (Phe) residues, its intrinsic fluorescence is mainly due to tryptophan [64]. The fluorescence intensity of protein was quenched through the addition of the synthesized complexes. This implies that the complexes strongly interact with HSA, leading to changes of microenvironment around the Trp-214 residue in HSA [59], [65]. Fig. 11 represents the fluorescence quenching of 3×10^{-6} M HSA at the presence of various amount of the complexes (5×10^{-5} M) at 298 K.

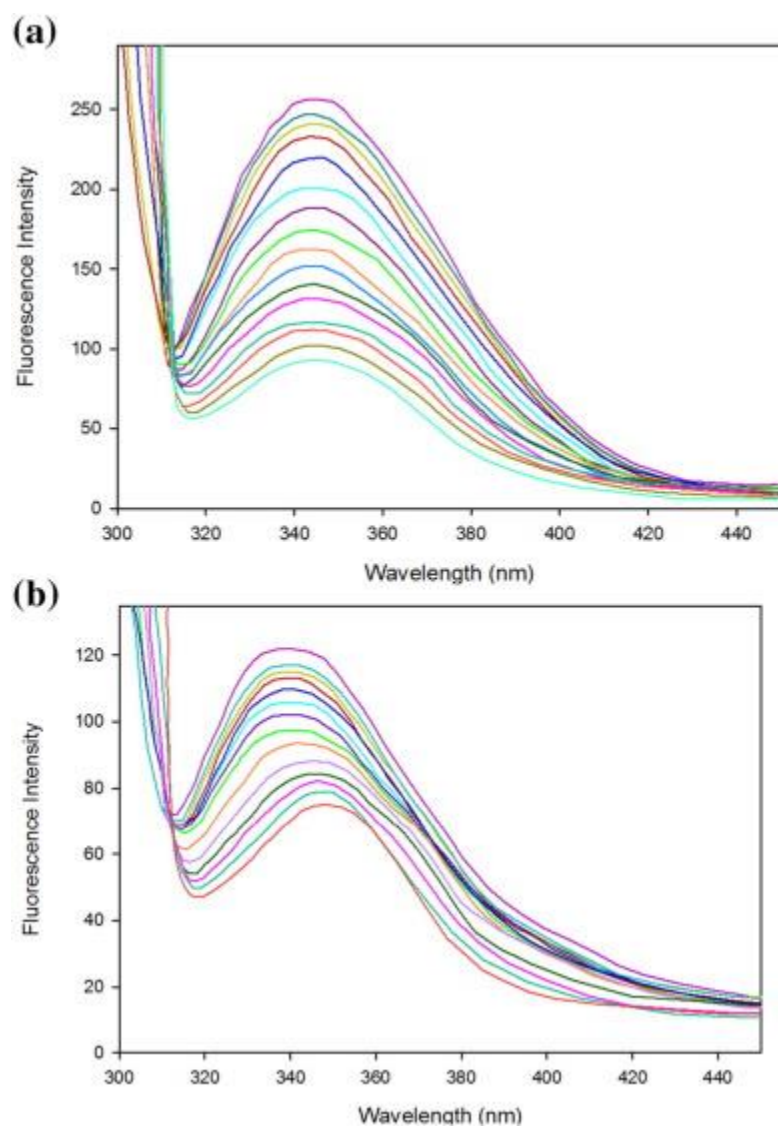


Fig. 11. Fluorescence spectra for titration of HSA (3×10^{-6} M) with increasing amounts of a) **PdL₂¹** and b) **PdL₂²** (5×10^{-5} M), $\lambda_{\text{ex}} = 295$ nm.

The absorptions of the complexes at the excitation and emission wavelengths were approximately zero in all concentrations. Hence, a reduction in the emission intensity is independent of the inner filter effect. In order to determine the binding ability between the complexes and HSA, the Stern–Volmer quenching plot was obtained by monitoring the fluorescence quenching of HSA with increasing the concentration of the complexes at different temperatures according to the Stern–Volmer equation [59]:

$$\frac{F_0}{F} = 1 + K_{\text{sv}}[\text{Q}] = 1 + k_{\text{q}}\tau[\text{Q}] \quad (4)$$

Where, F_0 and F are the fluorescence intensity of HSA in absence and presence of the complexes. K_{SV} is the Stern–Volmer quenching constant, k_{q} is the quenching rate constant of HSA and τ is the average lifetime of HSA without quencher which is typically equal to 10^{-8} s for biomacromolecules [26]. K_{SV} is determined from the plot of F_0/F vs. $[\text{Q}]$ at 298, 308 and 318 K (Fig. S1). In the present study, the value of K_{SV} was obtained and presented in Table 5.

Table 5. The HSA-binding constant (K_{b}), the number of binding site (n), the Stern–Volmer constant (K_{SV}) of the compounds and the quenching rate constant of HSA (k_{q}).

Compounds	T (K)	$K_{\text{b}}/\text{M}^{-1}$	n	$K_{\text{sv}}/\text{M}^{-1}$	$k_{\text{q}}/\text{M}^{-1}\cdot\text{S}^{-1}$
PdL₂¹	298	6.2×10^4	0.9	5.1×10^4	5.1×10^{12}
	308	2.0×10^5	0.75	1.0×10^5	1.0×10^{12}
	318	3.3×10^5	0.6	1.2×10^5	1.2×10^{12}
PdL₂²	298	3.3×10^4	0.91	1.9×10^4	1.9×10^{12}
	308	1.2×10^5	0.8	2.5×10^4	2.5×10^{12}
	318	1.6×10^5	0.5	6.1×10^4	6.1×10^{12}

Fluorescence quenching is classified to two mechanisms: static quenching and dynamic quenching. In the static mechanism, the fluorophore and the quencher collide together in the ground state while fluorophore and quencher collide together in the excited state in dynamic

mechanism. Linearity of the Stern–Volmer plot indicates that quenching fluorescence has only one mechanism, dynamic or static [26]. In this study, the value of K_{SV} increases with increasing temperature. This observation supports that quenching fluorescence of HSA occurs by dynamic mechanism [66].

Moreover, the binding constant (K_b) have been determined using the following equation at three temperatures [67]:

$$\text{Ln}\left(\frac{F_0-F}{F}\right) = \text{Ln}(K_b) + n\text{Ln}[Q] \quad (5)$$

[Q] is the concentration of quencher that is the synthesized complexes here. “ K_b ” is obtained from the plot of $\text{Ln}((F_0 - F)/F)$ versus $\text{Ln}[Q]$ as a y-intercept (Fig. S2). Furthermore, “ n ” which is the number of binding site per protein is slope of the plot [22]. The value of n is nearly 1, indicating that the synthesized complexes bind to HSA with molar ratio of 1:1. The calculated results are shown in Table 5. This result is in good agreement with the UV–vis spectroscopy result.

In general, binding constant of a drug with a carrier protein such as HSA should be high enough to bind and transfer thought body. Moreover, in order to release a drug since arrival at its target, it should not be too high. With respect to above, HSA Binding constants of the complexes is in a good range ($2-10 \times 10^4 \text{ M}^{-1}$) [68]. The Pd(II) complexes are in the uncharged form which is an advantage for a drug. Because the researches show that the unionized drugs are soluble in lipid and capable of crossing through the membrane's lipid bilayer while the ionized analogue species fail to cross [69].

3.5.3. Determination of the Thermodynamic Parameters

The main forces between a ligand and biomacromolecules include hydrophobic force, hydrogen bond, van der Waals force and electrostatic interactions [70]. Ross and Subramanian have used the sign and magnitude of the thermodynamic parameters (enthalpy change (ΔH), entropy change (ΔS) and free energy change (ΔG)) to determination of the type of these non-covalent interactions in a variety of host guest systems [71]. From the thermodynamic standpoint, $\Delta H > 0$ and $\Delta S > 0$ imply a hydrophobic interaction; $\Delta H < 0$ and $\Delta S < 0$ reflect the van der Waals force or hydrogen bond formation; and $\Delta H \approx 0$ and $\Delta S > 0$ suggestive of electrostatic forces [72]. The values of ΔH and ΔS are obtained from the van't Hoff equation [72]:

$$\ln K_b = -\frac{\Delta H}{RT} + \frac{\Delta S}{R} \quad (6)$$

Where K_b is the binding constant at the corresponding temperature, T is the absolute temperature in Kelvin and R is the gas constant. The values of ΔH and ΔS can be determined from the linear relationship between $\ln K_b$ and the reciprocal absolute temperature. ΔG can be evaluated from the following equation [72]:

$$\Delta G = \Delta H - T\Delta S \quad (7)$$

Table 6 lists the values of ΔG , ΔH and ΔS . In the present case, the enthalpic change > 0 and the entropic change > 0 , indicating the hydrophobic interaction is main force in the binding of the Pd(II) complexes to HSA. The value of ΔG is negative, so the binding process is spontaneous. The positive sign for ΔH shows the binding process is mainly an endothermic reaction.

Table 6. Thermodynamic parameters of **PdL₂¹** and **PdL₂²** with HSA.

Compounds	T (K)	ΔG (kJ·mol ⁻¹)	ΔH (kJ·mol ⁻¹)	ΔS (J·mol ⁻¹ ·K ⁻¹)
PdL₂¹	298	- 27.34	65.83	313.67
	308	- 31.27		
	318	- 33.59		
PdL₂²	298	- 25.78	63.66	300.71
	308	- 29.95		
	318	- 31.68		

As can be seen in Table 6 the spontaneity of complex–HSA binding reaction increases with increasing the temperature from 297 to 318 K.

3.5.4. Circular dichroism (CD) Spectroscopy

CD spectral technique is very effective to diagnose alteration on the secondary structure of HSA causing from HSA–drug interactions and also to investigate the conformation of protein quantitatively. The CD spectroscopy was performed in the absence and presence of the Pd(II) complexes to prove the impact of these complexes on the secondary structure of HSA. The CD spectra of HSA exhibits two negative peaks at 208 and 222 nm which are characteristic absorption peaks of α -helical structure of protein attributed to the $n\text{-}\pi^*$ transfer for the bonds of the α -helix [73]. The band intensities of HSA decreased in negative ellipticity upon the binding of the synthesized complexes to HSA, which indicates the decrease of the α -helical content and increase of disorder structure and β -sheet contents of HSA. This is the result of the formation complex between HSA and the complexes. The CD results can be expressed in terms of the mean residue ellipticity (MRE) according to Eq. (8)[73]:

$$\text{MRE} = \frac{\text{Observed CD (m degree)}}{C_p \cdot l} \times 10 \quad (8)$$

Where, C_p is the molar concentration of protein, l is the path length (0.1 cm), n is the number of amino acid residues that is 585 for HSA. The α -helical contents of free and combined HSA can be calculated from MRE values at 208 nm using the following equation:

$$\alpha - \text{helix}(\%) = \frac{-\text{MRE}_{208} - 4000}{33000 - 4000} \times 100 \quad (9)$$

Where, MRE_{208} is the observed mean residue ellipticity value at 208 nm, 4000 is the MRE of the β -sheet and random coil conformation cross at 208, and 33,000 is the MRE value of the pure α -helix at 208 nm. The contents of different secondary structures in HSA are presented in Table 7. Table 7. Changes in the secondary structure of HSA upon its interaction with the synthesized compounds in different concentration ($R = [\text{compound}] / \text{HSA}$).

R	HSA	HSA + PdL ₂ ¹				HSA + PdL ₂ ²		
	0	0.5	1	2	0.5	1	2	
α -Helix	58.6	39.7	34.9	32.8	33.4	30.8	24.7	

R	HSA	HSA + PdL ₂ ¹				HSA + PdL ₂ ²		
	0	0.5	1	2	0.5	1	2	
β-Sheet	21.0	26.4	29.3	31.1	30.2	34.9	44.6	
Random coil	19.7	35.6	23.9	23.4	34.4	34.9	40.1	

As it can be seen, the percentage of α -helix of HSA decreased while those of random coil and β -sheet increased. These results indicate that the complexes bound to the amino acid residues of the main polypeptide chain of HSA that causes destroy the original hydrogen bonding networks [74].

3.5.5. Energy Transfer from HSA to Complexes

Energy transfer between the compounds and HSA can provide valuable information about HSA-complex binding. The fluorescence quenching of HSA upon its binding to metal complex can be indicative of energy transfer between HSA and metal complex. This energy transfer can be explained by fluorescence resonance energy transfer (FRET) theory. FRET also known as Förster's resonance energy transfer which is an interaction between the excited molecule and its adjacent molecule. Upon this interaction, energy absorbed by donor molecule is transferred to an acceptor [75]. According to this theory, three conditions are required to energy transfer: (1) the donor should have fluorescence, (2) the fluorescence emission spectrum of the donor and the UV-vis spectrum of the acceptor should have sufficient overlap (3) the small distance between donor and acceptor (< 8 nm) [75]. The distance and efficiency of energy transfer (E) between tryptophan residue of protein (HSA) and drug (complex) has been calculated using this theory through the following equation:

$$E = 1 - \frac{F}{F_0} = \frac{R_0^6}{R_0^6 + r^6} \quad (10)$$

Where R_0 is the critical distance when the transfer efficiency is 50%; r is the distance between donor and acceptor. R_0 can be calculated by Eq. (11)[76].

$$R_0^6 = 8.79 \times 10^{-25} K^2 N^{-4} J \varphi \quad (11)$$

In the above equation, the term K^2 is the orientation factor of the dipoles; N is the refracted index of medium, J is the overlap integral of the fluorescence spectrum of the donor with absorption spectrum of the acceptor and ϕ is the fluorescence quantum yield of the donor. The value of J can be calculated by the following expression:

$$J = \frac{\sum F(\lambda)\varepsilon(\lambda)\lambda^4\Delta\lambda}{\sum F(\lambda)\Delta\lambda} \quad (12)$$

Where, $F(\lambda)$ is the fluorescence intensity of the donor in the absence of the acceptor at wavelength λ and ε is the molar absorption coefficient of the acceptor at λ . In the present case, $K^2 = 2/3$, $N = 1.336$ and $\phi = 0.15$ for HSA. Therefore, according to Eqs. (10), (11), (12) the parameters for the synthesized complexes were calculated (Table 8).

Table 8. The obtained results from FRET theory for the compounds.

Compounds	J ($\text{cm}^3 \cdot \text{L} \cdot \text{mol}^{-1}$)	R_0 (nm)	r (nm)	E
PdL₂¹	1.5×10^{-18}	0.59	0.60	0.46
PdL₂²	3.7×10^{-20}	0.32	0.31	0.52

Fig. 12 represents the overlap of the fluorescence emission spectrum of HSA (3 μM) and the UV–vis spectrum of complexes (3 μM). The values of r for the complexes are < 8 nm and $0.5 R_0 < r < 1.5 R_0$, suggesting energy transfer from HSA to them occurs with high probability [77].

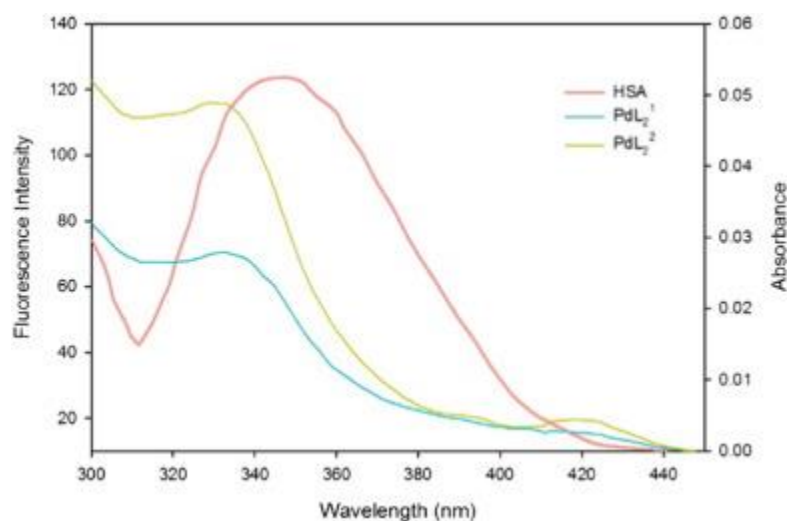


Fig. 12. Spectral overlap of the absorption spectra of the complexes with the HSA fluorescence.

3.5.6. Molecular Docking of the Pd(II) Complexes with HSA

In this work, the Pd(II) complexes were docked to the crystal structure of HSA (Fig. 13). As the Fig. 13 shows, the Pd(II) complexes bind to the IIB subdomain of HSA. The results indicated that ARG209, GLU208, SER480, GLU479 hydrophilic amino acid residues and ALA350, LEU347, ALA213, VAL482, LEU481, PHE206, GLY207, ALA210 hydrophobic amino acid residues are involved in the interaction with the **PdL₂¹**-HSA. Moreover, the **PdL₂²** complex interacts with ARG209, SER232 and ALA350, LEU327, VAL325, GLY328, LEU321, VAL216, VAL235, PHE228, LYS212, ASB324 hydrophilic and hydrophobic amino acid residues, respectively. In the **PdL₂¹**-HSA system PHE206 formed T-shaped π - π interaction. While there is a hydrogen bond with ASB324, a π -cation with LYS212 and two T-shaped π - π interactions with PHE228 in the **PdL₂²**-HSA system.

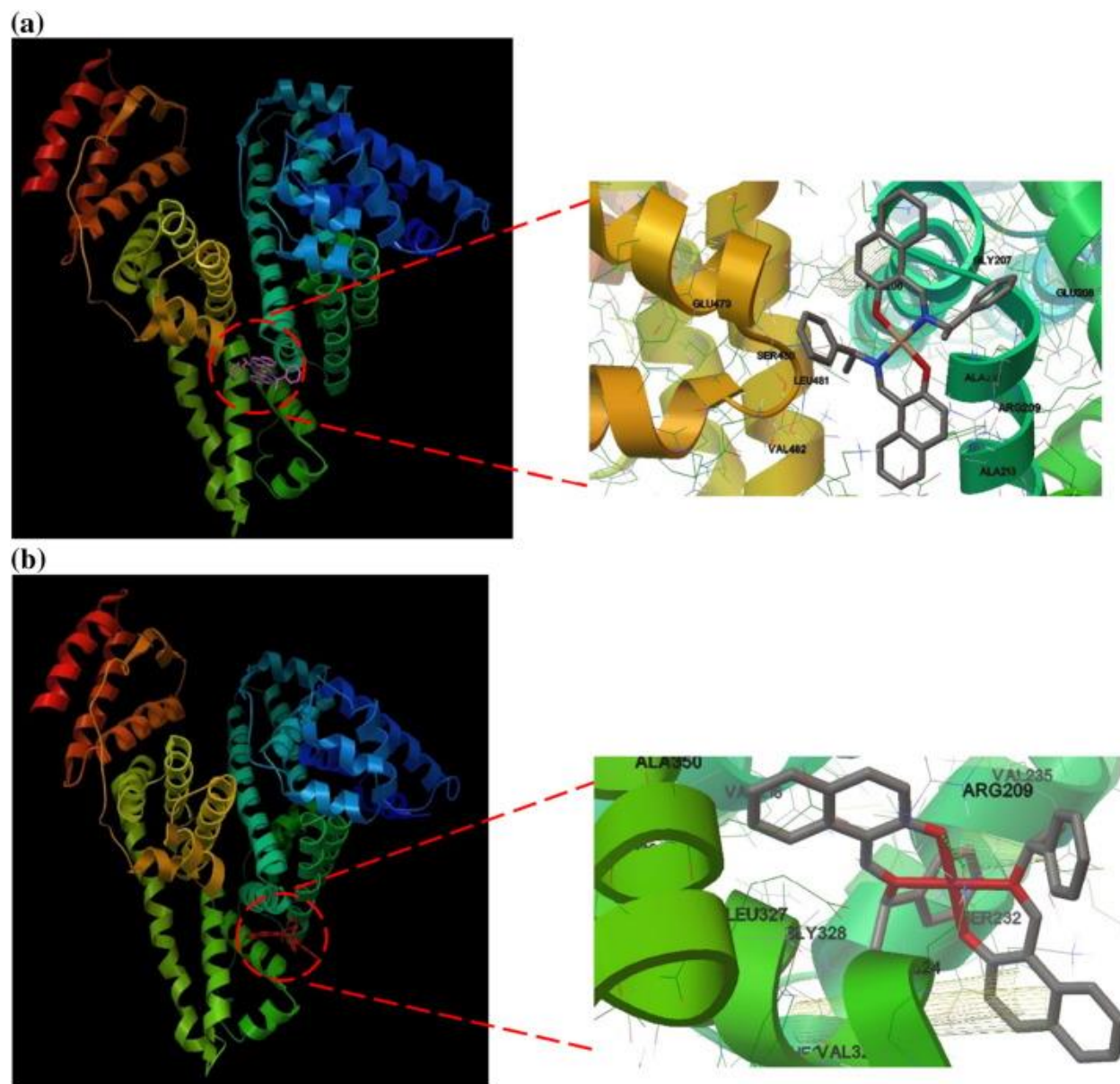


Fig. 13. The docking pose of a) PdL_2^1 -HSA and b) PdL_2^2 -HSA system.

The binding energy for PdL_2^1 and PdL_2^2 are evaluated about -8.73 and $-8.33 \text{ kcal}\cdot\text{mol}^{-1}$, respectively. The larger negative value of binding energy for PdL_2^1 means the higher affinity of it which is in a good agreement with experimental data.

As a result, the theoretical and experimental data show slight and considerable difference between binding constants of two diastereomers with HSA and DNA, respectively.

4. Conclusion

In the current study, synthesis of novel Pd(II) complexes from a racemic mixture ligand has been described. The resultant product is mixture of homochiral (*R,R/S,S*) and heterochiral (*R,S*) diastereomers which are in racemic and *meso* forms, respectively. The separation of these diastereomers has been accomplished by crystallization and then ¹H NMR technique with reliable results was used to investigate. Furthermore, the structure of *meso* diastereomers, **PdL₂¹**, was determined by single-crystal X-ray analysis. The crystallographic data show a square planar *trans*-[MN₂O₂] coordination geometry for them.

The DNA-binding of the synthesized complexes was also investigated, using fluorescence quenching, UV–vis spectroscopy, viscosity measurements and molecular docking. In addition, MCR-ALS, a powerful chemometrics method was carried out to study DNA-binding of complexes, quantitatively. It can be found that both diastereomers interact with DNA, presumably by the groove binding mechanism. According to these results, **PdL₂¹** exhibited stronger DNA binding affinity compared to **PdL₂²**.

The experimental (fluorescence quenching, UV–vis spectroscopy and circular dichroism) and computational methods (molecular docking) were carried out to study HSA-binding of the complexes. Circular dichroism spectroscopy was used to investigate the changes on the secondary structure of HSA upon its interaction with the complexes. The obtained results from this spectroscopy indicate that the percentage of α -helix of HSA decreased while those of random coil and β -sheet increased upon addition of the synthesized complexes to HSA. In addition, the sign and magnitude of the thermodynamic parameters (ΔH , ΔS and ΔG) indicate that the main acting force between HSA and both diastereomers is hydrophobic force.

As a conclusion, the binding constant of two diastereomers with HSA and DNA have slight and considerable difference, respectively.

Appendix A. Supplementary data

Supplementary data to this article can be found online at <http://dx>.

doi.org/10.1016/j.jphotobiol.2016.08.035.

References

[1] B.B. Aggarwal, D. Danda, S. Gupta, P. Gehlot, Models for prevention and treatment of

cancer: problems vs promises, *Biochem. Pharmacol.* 78 (2009) 1083–1094.

[2] Shipra Yadav, Imtiyaz Yousuf, Mohammad Usman, Musheer Ahmad, Farukh Arjmand, Sartaj Tabassum, Synthesis and spectroscopic characterization of diorganotin(IV) complexes of N'-(4-hydroxypent-3-en-2-ylidene)isonicotinohydrazide: chemotherapeutic potential validation by in vitro interaction studies with DNA/HSA, DFT, molecular docking and cytotoxic activity, *RSC Adv.* 5 (2015) 50673–50690.

[3] K.W. Wellington, Understanding cancer and the anticancer activities of naphthoquinones—a review, *RSC Adv.* 5 (2015) 20309–20338.

[4] M. Carreira, R. Calvo-Sanjuán, M. Sanaú, X. Zhao, R.S. Magliozzo, I. Marzo, M. Contel, Cytotoxic hydrophilic iminophosphorane coordination compounds of d 8 metals. Studies of their interactions with DNA and HSA, *J. Inorg. Biochem.* 116 (2012) 204–214.

[5] L. Yan, X. Wang, Y. Wang, Y. Zhang, Y. Li, Z. Guo, Cytotoxic palladium(II) complexes of 8-aminoquinoline derivatives and the interaction with human serum albumin, *J. Inorg. Biochem.* 106 (2012) 46–51.

[6] T.V. Serebryanskaya, T. Yung, A.A. Bogdanov, A. Shchebet, S.A. Johnsen, A.S. Lyakhov, L.S. Ivashkevich, Z.A. Ibrahimava, T.S. Garbuzenco, T.S. Kolesnikova, Synthesis, characterization, and biological evaluation of new tetrazole-based platinum (II) and palladium (II) chlorido complexes—potent cisplatin analogues and their trans isomers, *J. Inorg. Biochem.* 120 (2013) 44–53.

[7] E.S. Koumoussi, M. Zampakou, C.P. Raptopoulou, V. Psycharis, C.M. Beavers, S.J. Teat, G. Psomas, T.C. Stamatatos, First palladium (ii) and platinum (ii) complexes from employment of 2, 6-diacetylpyridine dioxime: synthesis, structural and spectroscopic characterization, and biological evaluation, *Inorg. Chem.* 51 (2012) 7699–7710.

[8] R. Prabhakaran, P. Kalaivani, P. Poornima, F. Dallemer, R. Huang, V.V. Padma, K. Natarajan, Synthesis, DNA/protein binding and in vitro cytotoxic studies of new palladium metallothiosemicarbazones, *Bioorg. Med. Chem.* 21 (2013) 6742–6752.

[9] W.M. Motswainyana, M.O. Onani, A.M. Madiehe, M. Saibu, N. Thovhogi, R.A.

Lalancette, Imino-phosphine palladium (II) and platinum (II) complexes: synthesis, molecular structures and evaluation as antitumor agents, *J. Inorg. Biochem.* 129 (2013) 112–118.

[10] N.J. Wheate, S. Walker, G.E. Craig, R. Oun, The status of platinum anticancer drugs in the clinic and in clinical trials, *Dalton Trans.* 39 (2010) 8113–8127.

[11] C.-H. Ng, W.-S. Wang, K.-V. Chong, Y.-F. Win, K.-E. Neo, H.-B. Lee, S.-L. San, R.N.Z.R.A. Rahman, W.K. Leong, Ternary copper (II)-polypyridyl enantiomers: aldol-type condensation, characterization, DNA-binding recognition, BSA-binding and anticancer property, *Dalton Trans.* 42 (2013) 10233–10243.

[12] W.I. Sundquist, D.P. Bancroft, S.J. Lippard, Synthesis, characterization, and biological activity of cis-diammineplatinum (II) complexes of the DNA intercalators 9-aminoacridine and chloroquine, *J. Am. Chem. Soc.* 112 (1990) 1590–1596.

[13] S. Tabassum, A. Asim, R.A. Khan, Z. Hussain, S. Srivastav, S. Srikrishna, F. Arjmand, Chiral heterobimetallic complexes targeting human DNA-topoisomerase α , *Dalton Trans.* 42 (2013) 16749–16761.

[14] N.-u.H. Khan, N. Pandya, K.J. Prathap, R.I. Kureshy, S.H.R. Abdi, S. Mishra, H.C. Bajaj, Chiral discrimination asserted by enantiomers of Ni (II), Cu (II) and Zn (II) Schiff base complexes in DNA binding, antioxidant and antibacterial activities, *Spectrochim. Acta A Mol. Biomol. Spectrosc.* 81 (2011) 199–208.

[15] L.A. Nguyen, H. He, C. Pham-Huy, Chiral drugs: an overview, *Int. J. Biomed. Sci.* 2 (2006) 58–100.

[16] Y. Dong, Q. Shi, Y.-N. Liu, X. Wang, K.F. Bastow, K.-H. Lee, Antitumor agents. 266. Design, synthesis, and biological evaluation of novel 2-(furan-2-yl)naphthalen-1-ol derivatives as potent and selective antibreast cancer agents, *J. Med. Chem.* 52 (2005) 3586–3590.

[17] M.I. Dawson, P.D. Hobbs, V.J. Peterson, M. Leid, C.W. Lange, K.-C. Feng, G.-q. Chen, H.L. Jian Gu, S.K. Kolluri, X.-k. Zhang, Y. Zhang, J.A. Fontana, Apoptosis induction in cancer cells by a novel analogue of 6-[3-(1-adamantyl)-4-hydroxyphenyl]-2-naphthalenecarboxylic acid lacking retinoid receptor transcriptional activation activity, *Cancer Res.* 61 (2001) 4723–4730.

- [18] K.J. Kilpin, C.M. Clavel, F. Edafe, P.J. Dyson, Naphthalimide-tagged ruthenium–arene anticancer complexes: combining coordination with intercalation, *Organometallics* 31 (2012) 7031–7039.
- [19] M. Wasowska-Lukawska, J. Wietrzyk, A. Opolski, J. Oszczapowicz, I. Oszczapowicz, Biological properties of new derivatives of daunorubicin, *In Vivo*. 21 (2007) 413–416.
- [20] P. Rani, D. Pal, R.R. Hegde, S.R. Hashim, Anticancer, anti-inflammatory, and analgesic activities of synthesized 2-(substituted phenoxy) acetamide derivatives, *BioMed Res. Int.* 2014 (2014).
- [21] J. Jaumot, R. Gargallo, A. de Juan, R. Tauler, A graphical user-friendly interface for MCR-ALS: a new tool for multivariate curve resolution in MATLAB, *Chemom. Intell. Lab. Syst.* 76 (2005) 101–110.
- [22] S. Cie, Program for the Acquisition and Analysis of Data XeAREA, Version 1.30, Stoe & Cie GmbH, Darmstadt, Germany, 2005.
- [23] Stoe&Cie, Program for Crystal Optimization for Numerical Absorption Correction Xe; SHAPE, S.C. GmbH, Darmstadt, Germany, 2004.
- [24] M.C. Burla, R. Caliandro, M. Camalli, B. Carrozzini, G.L. Cascarano, L. De Caro, C. Giacovazzo, G. Polidori, R. Spagna, SIR2004: an improved tool for crystal structure determination and refinement, *J. Appl. Crystallogr.* 38 (2005) 381–388.
- [25] K. Zheng, F. Liu, X.-M. Xu, Y.-T. Li, Z.-Y. Wu, C.-W. Yan, Synthesis, structure and molecular docking studies of dicopper (II) complexes bridged by N-phenolato-N'-[2-(dimethylamino) ethyl] oxamide: the influence of terminal ligands on cytotoxicity and reactivity towards DNA and protein BSA, *New J. Chem.* 38 (2014) 2964–2978.
- [26] Z. Kazemi, H. Amiri Rudbari, V. Mirkhani, M. Sahihi, M. Moghadam, S. Tangestaninejad, I. Mohammadpoor-Baltork, Synthesis, characterization, crystal structure, DNA- and HSA-binding studies of a dinuclear Schiff base Zn (II) complex derived from 2-hydroxynaphthaldehyde and 2-picolylamine, *J. Mol. Struct.* 1096 (2015) 110–120.
- [27] M.J. Frisch, G.W. Trucks, H.B. Schlegel, G.E. Scuseria, J.R.C.M.A. Robb, G. Scalmani, V. Barone, G.A.P.B. Mennucci, H. Nakatsuji, M. Caricato, H.P.H.X. Li, A.F. Izmaylov, J.

Bloino, G. Zheng, M.H.J.L. Sonnenberg, M. Ehara, K. Toyota, J.H.R. Fukuda, M. Ishida, T. Nakajima, Y. Honda, H.N.O. Kitao, T. Vreven, J.A. Montgomery Jr., F.O.J.E. Peralta, M. Bearpark, J.J. Heyd, K.N.K.E. Brothers, V.N. Staroverov, R. Kobayashi, K.R.J. Normand, A. Rendell, J.C. Burant, J.T.S.S. Iyengar, M. Cossi, N. Rega, J.M. Millam, J.E.K.M. Klene, J.B. Cross, V. Bakken, C. Adamo, R.G.J. Jaramillo, R.E. Stratmann, O. Yazyev, R.C.A.J. Austin, C. Pomelli, J.W. Ochterski, K.M.R.L. Martin, V.G. Zakrzewski, G.A. Voth, J.J.D.P. Salvador, S. Dapprich, A.D. Daniels, J.B.F.O. Farkas, J.V. Ortiz, J. Cioslowski, D.J. Fox, Revision B.01, Gaussian Development Version, Gaussian. Inc., Wallingford, CT, 2009.

[28] G.M. Morris, D.S. Goodsell, R.S. Halliday, R. Huey, W.E. Hart, R.K. Belew, A.J. Olson, Automated docking using a Lamarckian genetic algorithm and an empirical binding free energy function, *J. Comput. Chem.* 19 (1998) 1639–1662.

[29] M. Enamullah, A.R. Uddin, G. Pescitelli, R. Berardozi, G. Makhloufi, V. Vasylyeva, A.-C. Chamayou, C. Janiak, Induced chirality-at-metal and diastereoselectivity at Δ/Λ -configured distorted square-planar copper complexes by enantiopure Schiff base ligands: combined circular dichroism, DFT and X-ray structural studies, *Dalton Trans.* 43 (2014) 3313–3329.

[30] A.-C. Chamayou, S. Lüdeke, V. Brecht, T.B. Freedman, L.A. Nafie, C. Janiak, Chirality and diastereoselection of Δ/Λ -configured tetrahedral zinc complexes through enantiopure Schiff Base complexes: combined vibrational circular dichroism, density functional theory, ^1H NMR, and X-ray structural studies, *Inorg. Chem.* 50 (2011) 11363–11374.

[31] M. Enamullah, V. Vasylyeva, C. Janiak, Chirality and diastereoselection of Δ/Λ -configured tetrahedral zinc (II) complexes with enantiopure or racemic Schiff base ligands, *Inorg. Chim. Acta* 408 (2013) 109–119.

[32] T. Atta-Ur-Rahman, *Nuclear Magnetic Resonance: Basic Principles*, Springer Science & Business Media, 2012.

[33] R.R. Coombs, M.K. Ringer, J.M. Blacquiere, J.C. Smith, J.S. Neilsen, Y.-S. Uh, J.B. Gilbert, L.J. Leger, H. Zhang, A.M. Irving, Palladium (II) Schiff base complexes derived from sulfanilamides and aminobenzothiazoles, *Transit. Met. Chem.* 30 (2005) 411–418.

- [34] M. Khorshidifard, H. Amiri Rudbari, B. Askari, M. Sahihi, M.R. Farsani, F. Jalilian, G. Bruno, Cobalt (II), copper (II), zinc (II) and palladium (II) Schiff base complexes: synthesis, characterization and catalytic performance in selective oxidation of sulfides using hydrogen peroxide under solvent-free conditions, *Polyhedron* 95 (2015) 1–13.
- [35] M. Khorshidifard, H. Amiri Rudbari, Z. Kazemi-Delikani, V. Mirkhani, R. Azadbakht, Synthesis, characterization and X-ray crystal structures of vanadium (IV), cobalt (III), copper (II) and zinc (II) complexes derived from an asymmetric bidentate Schiff-base ligand at ambient temperature, *J. Mol. Struct.* 1081 (2015) 494–505.
- [36] H. Bahron, A.M. Tajuddin, W.N.W. Ibrahim, S. Chantrapromma, H.-K. Fun, Bis {2-methoxy-6-[(E)-(4-methylbenzyl) iminomethyl] phenolato} palladium (II) chloroform monosolvate, *Acta Crystallogr., Sect. E* 70 (2014) m289–m290.
- [37] O.A. Blackburn, B.J. Coe, J. Fielden, M. Helliwell, J.J. McDouall, M.G. Hutchings, Nickel (II) and palladium (II) complexes of Azobenzene-containing ligands as dichroic dyes, *Inorg. Chem.* 49 (2010) 9136–9150.
- [38] Z. Gan, K. Kawamura, K. Eda, M. Hayashi, Effect of ortho-substituents on the stereochemistry of 2-(o-substituted phenyl)-1H-imidazoline–palladium complexes, *J. Organomet. Chem.* 695 (2010) 2022–2029.
- [39] A.W. Maverick, R.K. Laxman, M.A. Hawkins, D.P. Martone, F.R. Fronczek, Flexible cofacial binuclear metal complexes derived from α , α -bis (salicylimino)-m-xylene, *Dalton Trans.* (2005) 200–206.
- [40] U. Caruso, R. Diana, B. Panunzi, A. Roviello, M. Tingoli, A. Tuzi, Facile synthesis of new Pd (II) and Cu (II) based metallomesogens from ligands containing thiophene rings, *Inorg. Chem. Commun.* 12 (2009) 1135–1138.
- [41] M. Sirajuddin, S. Ali, A. Badshah, Drug–DNA interactions and their study by UV–visible, fluorescence spectroscopies and cyclic voltametry, *J. Photochem. Photobiol. B* 124 (2013) 1–19.
- [42] K. Abdi, H. Hadadzadeh, M. Weil, H. Amiri Rudbari, Mono- and polynuclear copper (II) complexes based on 2, 4, 6-tris (2-pyridyl)-1, 3, 5-triazine and its hydrolyzed

form, *Inorg. Chim. Acta* 416 (2014) 109–121.

[43] S. Kathiresan, S. Mugesh, M. Murugan, F. Ahamed, J. Annaraj, Mixed-ligand copper (ii)-phenolate complexes: structure and studies on DNA/protein binding profiles, DNA cleavage, molecular docking and cytotoxicity, *RSC Adv.* 6 (2016) 1810–1825.

[44] F. Arjmand, A. Jamsheera, DNA binding studies of new valine derived chiral complexes of tin (IV) and zirconium (IV), *Spectrochim. Acta A* 78 (2011) 45–51.

[45] P. Awasthi, N. Kumar, R. Kaushal, M. Kumar, S. Kukreti, Comparative in vitro binding studies of $TiCl_2(dpme)_2$, $Ti(ada)_2(bzac)_2$, and $TiCl_2(bzac)(bpme)$ titanium complexes with calf-thymus DNA, *Biochem Res. Int.* 2015 (2015).

[46] P. Kalaivani, R. Prabhakaran, F. Dallemer, P. Poornima, E. Vaishnavi, E. Ramachandran, V.V. Padma, R. Renganathan, K. Natarajan, DNA, protein binding, cytotoxicity, cellular uptake and antibacterial activities of new palladium (II) complexes of thiosemicarbazone ligands: effects of substitution on biological activity, *Metallomics* 4 (2012) 101–113.

[47] M. Kalita, K.J. Tamuli, P. Barman, B. Sarma, R. Baruah, H.P.D. Boruah, Synthesis, crystal structure, bioactivities of Ni (II), Cu (II), Co (II) and Pd (II) complexes with unsymmetrical thioether donor Schiff base: phosphine free Pd (II) complex catalyzed Suzuki reaction, *Polyhedron* 97 (2015) 140–147.

[48] S.S. Bhat, A.A. Kumbhar, H. Heptullah, A.A. Khan, V.V. Gobre, S.P. Gejji, V.G. Puranik, Synthesis, electronic structure, DNA and protein binding, DNA cleavage, and anticancer activity of fluorophore-labeled copper (II) complexes, *Inorg. Chem.* 50 (2010) 545–558.

[49] X. Zhou, G. Zhang, J. Pan, Groove binding interaction between daphnetin and calf thymus DNA, *Int. J. Biol. Macromol.* 74 (2015) 185–194.

[50] Q. Zhang, Y. Wang, Y. Ni, S. Kokot, Analysis of complex molecular systems: the impact of multivariate analysis for resolving the interactions of small molecules with biopolymers—a review, *Anal. Lett.* 47 (2014) 1089–1106.

[51] X. Zhou, C. Zhang, G. Zhang, Y. Liao, Intercalation of the daphnetin–Cu (II) complex with calf thymus DNA, *RSC Adv.* 6 (2016) 5408–5418.

- [52] Y. Li, G. Zhang, M. Tao, Binding properties of herbicide chlorpropham to DNA: spectroscopic, chemometrics and modeling investigations, *J. Photochem. Photobiol. B* 138 (2014) 109–117.
- [53] Y.-H. Liu, A. Li, J. Shao, C.-Z. Xie, X.-Q. Song, W.-G. Bao, J.-Y. Xu, Four Cu (ii) complexes based on antitumor chelators: synthesis, structure, DNA binding/damage, HSA interaction and enhanced cytotoxicity, *Dalton Trans.* 45 (2016) 8036–8049.
- [54] M. Sahihi, Y. Ghayeb, A.-K. Bordbar, Fluorescence spectroscopic study on interaction of retinol with β -lactoglobulin in the presence of cetylpyridinium chloride, *J. Spectrosc.* 27 (2012) 27–34.
- [55] P. Kalaivani, R. Prabhakaran, E. Ramachandran, F. Dallemer, G. Paramaguru, R. Renganathan, P. Poornima, V.V. Padma, K. Natarajan, Influence of terminal substitution on structural, DNA, protein binding, anticancer and antibacterial activities of palladium (II) complexes containing 3-methoxy salicylaldehyde-4 (N) substituted thiosemicarbazones, *Dalton Trans.* 41 (2012) 2486–2499.
- [56] M.M. McCallum, A.J. Pawlak, W.R. Shadrack, A. Simeonov, A. Jadhav, A. Yasgar, D.J. Maloney, L.A. Arnold, A fluorescence-based high throughput assay for the determination of small molecule–human serum albumin protein binding, *Anal. Bioanal. Chem.* 406 (2014) 1867–1875.
- [57] F. Li, M. Feterl, J.M. Warner, A.I. Day, F.R. Keene, J.G. Collins, Protein binding by dinuclear polypyridyl ruthenium (II) complexes and the effect of cucurbit [10] uril encapsulation, *Dalton Trans.* 42 (2013) 8868–8877.
- [58] B. Demoro, R.F. de Almeida, F. Marques, C.P. Matos, L. Otero, J.C. Pessoa, I. Santos, A. Rodríguez, V. Moreno, J. Lorenzo, Screening organometallic binuclear thiosemicarbazone ruthenium complexes as potential anti-tumour agents: cytotoxic activity and human serum albumin binding mechanism, *Dalton Trans.* 42 (2013) 7131–7146.
- [59] E.M. Mrkalić, R.M. Jelić, O.R. Klisurić, Z.D. Matović, Synthesis of novel palladium (II) complexes with oxalic acid diamide derivatives and their interaction with nucleosides and proteins. Structural, solution, and computational study, *Dalton Trans.* 43 (2014) 15126–15137.

- [60] Z. Kazemi, H. Amiri Rudbari, M. Sahihi, V. Mirkhani, M. Moghadam, S. Tangestaninejad, I. Mohammadpoor-Baltork, S. Gharaghani, Synthesis, characterization and biological application of four novel metal-Schiff base complexes derived from allylamine and their interactions with human serum albumin: experimental, molecular docking and ONIOM computational study, *J. Photochem. Photobiol. B* 162 (2016) 448–462.
- [61] S.-L. Zhang, J.-J. Chang, G.L. Damu, R.-X. Geng, C.-H. Zhou, Berberine azoles as antimicrobial agents: synthesis, biological evaluation and their interactions with human serum albumin, *Med. Chem. Commun.* 4 (2013) 839–846.
- [62] A. Das, G.S. Kumar, Binding studies of aristololactam- β -D-glucoside and daunomycin to human serum albumin, *RSC Adv.* 4 (2014) 33082–33090.
- [63] H.K. Noor-ul, N. Pandya, N.C. Maity, M. Kumar, R.M. Patel, R.I. Kureshy, S.H. Abdi, S. Mishra, S. Das, H.C. Bajaj, Influence of chirality of V (V) Schiff base complexes on DNA, BSA binding and cleavage activity, *Eur. J. Med. Chem.* 46 (2011) 5074–5085.
- [64] M. Ganeshpandian, R. Loganathan, E. Suresh, A. Riyasdeen, M.A. Akbarsha, M. Palaniandavar, New ruthenium (II) arene complexes of anthracenyl-appended diazacycloalkanes: effect of ligand intercalation and hydrophobicity on DNA and protein binding and cleavage and cytotoxicity, *Dalton Trans.* 43 (2014) 1203–1219.
- [65] Y.-Q. Wang, H.-M. Zhang, G.-C. Zhang, W.-H. Tao, S.-H. Tang, Interaction of the flavonoid hesperidin with bovine serum albumin: a fluorescence quenching study, *J. Lumin.* 126 (2007) 211–218.
- [66] R.L. Joseph, R. Lakowicz, *Principles of Fluorescence Spectroscopy*, Kluwer Academic/Plenum Publishers, New York, 1999.
- [67] S.U. Dighe, S. Khan, I. Soni, P. Jain, S. Shukla, R. Yadav, P. Sen, S.M. Meeran, S. Batra, Synthesis of β -carboline-based N-heterocyclic carbenes and their antiproliferative and anti-metastatic activities against human breast cancer cells, *J. Med. Chem.* 58 (8) (2015) 3485–3499.
- [68] M. Kyropoulou, C.P. Raptopoulou, V. Psycharis, G. Psomas, Ni (II) complexes with non-steroidal anti-inflammatory drug diclofenac: structure and interaction with DNA and albumins, *Polyhedron* 61 (2013) 126–136.

- [69] O.K. Abou-Zied, Revealing the ionization ability of binding site I of human serum albumin using 2-(2'-hydroxyphenyl) benzoxazole as a pH sensitive probe, *Phys. Chem. Chem. Phys.* 14 (2012) 2832–2839.
- [70] J. Li, J. Li, Y. Jiao, C. Dong, Spectroscopic analysis and molecular modeling on the interaction of jatrorrhizine with human serum albumin (HSA), *Spectrochim. Acta A* 118 (2014) 48–54.
- [71] P.D. Ross, S. Subramanian, Thermodynamics of protein association reactions: forces contributing to stability, *Biochemistry* 20 (1981) 3096–3102.
- [72] S. Tabassum, M. Zaki, M. Ahmad, M. Afzal, S. Srivastav, S. Srikrishna, F. Arjmand, Synthesis and crystal structure determination of copper (II)-complex: in vitro DNA and HSA binding, pBR322 plasmid cleavage, cell imaging and cytotoxic studies, *Eur. J. Med. Chem.* 83 (2014) 141–154.
- [73] I. Khosravi, F. Hosseini, M. Khorshidifard, M. Sahihi, H. Amiri Rudbari, Synthesis, characterization, crystal structure and HSA binding of two new N, O, O-donor Schiff-base ligands derived from dihydroxybenzaldehyde and tert-butylamine, *J. Mol. Struct.* 1119 (2016) 373–384.
- [74] P. Banerjee, S. Ghosh, A. Sarkar, S.C. Bhattacharya, Fluorescence resonance energy transfer: a promising tool for investigation of the interaction between 1-anthracene sulphonate and serum albumins, *J. Lumin.* 131 (2011) 316–321.
- [75] N. Fani, A. Bordbar, Y. Ghayeb, A combined spectroscopic, docking and molecular dynamics simulation approach to probing binding of a Schiff base complex to human serum albumin, *Spectrochim. Acta, Part A* 103 (2013) 11–17.
- [76] F. Deng, Y. Liu, Study of the interaction between tosufloxacin tosylate and bovine serum albumin by multi-spectroscopic methods, *J. Lumin.* 132 (2012) 443–448.
- [77] X.-B. Fu, G.-T. Weng, D.-D. Liu, X.-Y. Le, Synthesis, characterization, DNA binding and cleavage, HSA interaction and cytotoxicity of a new copper (II) complex derived from 2-(2'-pyridyl) benzothiazole and glycylglycine, *J. Photochem. Photobiol., A* 276 (2014) 83–95.
- [78] J.L. Packer, J.J. Werner, D.E. Latch, K. McNeill, W.A. Arnold, Photochemical fate of pharmaceuticals in the environment: naproxen, diclofenac, clofibrilic acid, and ibuprofen, *Aquat. Sci.* 65 (2003) 342–351.

- [79] I. Hayakawa, S. Atarashi, S. Yokohama, M. Imamura, K. Sakano, M. Furukawa, Synthesis and antibacterial activities of optically active ofloxacin, *Antimicrob. Agents Chemother.* 29 (1986) 163–164.
- [80] G.L. Perlovich, T.V. Volkova, A. Bauer-Brandl, Thermodynamic study of sublimation, solubility, solvation, and distribution processes of atenolol and pindolol, *Mol. Pharm.* 4 (2007) 929–935.
- [81] T.H. Corbett, P. LoRusso, L. Demchick, C. Simpson, S. Pugh, K. White, J. Kushner, L. Polin, J. Meyer, J. Czarnecki, Preclinical antitumor efficacy of analogs of XK469: sodium-(2-[4-(7-chloro-2-quinoxalinyloxy) phenoxy] propionate), *Investig. New Drugs* 16 (1998) 129–139.
- [82] V.K. Prasad, S. Corlett, K. Abaasi, D. Heney, I. Lewis, H. Chrystyn, Ifosfamide enantiomers: pharmacokinetics in children, *Cancer Chemother. Pharmacol.* 34 (1994) 447–449.
- [83] K. Misiura, R.W. Kinas, W.J. Stec, H. Kusnierczyk, C. Radzikowski, A. Sonoda, Synthesis and antitumor activity of analogs of ifosfamidemodified in the N-(2-chloroethyl) group, *J. Med. Chem.* 31 (1988) 226–230.